공학박사 학위논문

3D 프린팅 기반 의료영상 및 현실적인 재료물성 개선을 통한 이미징 팬텀, 교육용 및 리허설 팬텀 제작과 임상적용에 관한 연구

Enhancement of medical imaging and realistic material property using 3D printing: application to imaging, education, and rehearsal phantoms

울산대학교 대학원
의 과 학 과
홍 다 영

3D 프린팅 기반 의료영상 및 현실적인 재료물성 개선을 통한 이미징 팬텀, 교육용 및 리허설 팬텀 제작과 임상적용에 관한 연구

지도교수 김 남 국

이 논문을 공학박사 학위 논문으로 제출함

2023 년 8 월

울산대학교 대학원

의 과 학 과

홍 다 영

홍다영의 공학박사 학위 논문을 인준함

심사위원장 이 상 민 (인)

심사위원 김 남 국 (인)

심사위원 고 범 석 (인)

심사위원 오 일 영 (인)

심사위원 유 진 수 (인)

울 산 대 학 교 대 학 원

2023 년 8 월

감사의 글

바쁘신 일정에도 저의 논문 심사에 기꺼이 참여해주시고 긍정적인 평가와 고견 주신 서울아산병원 이상민 교수님, 고범석 교수님, 삼성서울병원 유진수 교수님, 분당서울대병원 오일영 교수님께 진심으로 감사드립니다. 그리고 약 7 년 동안 MI2RL 연구실에서 다양한 연구에 도전하고 뜻깊은 성과를 이룰 수 있도록 독려해주시고 지지해주신 김남국 지도교수님께도 깊은 감사드립니다.

의료영상과 3D 프린팅을 주제로 박사졸업을 성공적으로 마칠 수 있도록 물심양면 도움주신 3D 프린팅팀 김태훈 박사, 옥준혁 선생님, 김현정선생님, 김지연선생님, 온성철선생님께도 감사드립니다. 뿐만 아니라 그 간 함께 수고해주신 MI2RL 연구실의 모든 교수님들, 연구원분들, 관리팀 선생님들께도 감사드립니다.

더불어 최종 목표를 향해 달릴 수 있게 항상 도움주시고 격려해주신 방사선학과 박명환 교수님, 김형균 교수님께도 감사드립니다. 교수님의 응원과 지지는 제가 지치지 않고 학문적으로 더 성장할 수 있는 큰 힘이 되었습니다.

마지막으로 항상 믿고 지지해주시는 사랑하는 부모님, 남편, 딸 시아, 그리고 늘 응원해주시고 이해해주신 시부모님과 양가 가족들께도 무한한 감사드립니다.

2023 년 여름,

홍다영 올림

Abstract

With the development and popularization of three-dimensional (3D) printing technology, it is being used in various ways in the medical field to overcome the limitations of existing technology. 3D printing can be manufactured without restrictions on the shape, and small-scale production is possible. In particular, complex shapes with porosity were difficult to manufacture with conventional manufacturing methods, but 3D printing made it possible. In addition, due to the manufacturing characteristics of 3D printing, it is suitable for small-quantity production of various kinds. Therefore, in medicine, it is possible to produce patient-specific and disease-specific medical devices.

Medical 3D printing has the potential to transform the way doctors diagnose and treat patients by providing customized solutions for complex surgeries and medical procedures. With the use of advanced medical imaging techniques, such as CT and MRI scans, 3D printing can produce highly accurate and realistic models of patients' anatomy. These models can be used to plan and rehearse surgeries, design custom implants or prosthetics, and create medical devices that are tailored to the individual patient's needs.

One of the benefits of 3D printing in the medical field is the ability to create realistic, patient-specific, and reusable phantoms. These phantoms can be used for challenging surgeries that have a low frequency of occurrence, allowing surgeons to practice and perfect their techniques before performing the actual surgery. This can lead to better outcomes for patients and a higher level of confidence for surgeons. It can also be used to evaluate medical imaging software.

The development of a CT-based pediatric video thoracoscopic simulation phantom showed effects such as improving the accuracy of surgery and shortening the operation time through pre-operative rehearsal simulation for patients and surgeons in operations with high difficulty

and low frequency. In addition, various Hounsfield units (HU) were implemented using medical imaging, 3D printing technology, and foamed silicone, and a chest phantom reflecting the pattern of the disease was fabricated and applied to quantification software evaluation. Lastly, the left atrial appendage occlusion rehearsal simulation phantom enabled more predictable and accurate surgery through pre-operative simulation.

In conclusion, medical imaging and 3D printing technologies realize highly customized technologies such as patient-specific and show new possibilities for innovative medical technologies. 3D printing technology improves the existing medical process to enable high-level medical care.

Key words: 3D Printing, Computed tomography, Imaging phantom, Medical image, Simulation

Contents

List of Tables

List of Figures

List of Abbreviations

3D	Three-dimensional
FDM	Fused deposition modeling
DLP	Digital Light Processing
UV	Ultraviolet
SLA	Stereolithography
CJP	ColorJet Printing
VATS	Video-assisted thoracoscopic surgery
EATEF	Esophageal atresia with or without tracheoesophageal fistula
CT	Computed tomography
STL	Stereolithrography
MRI	Magnetic Resonance Imaging
2D	Two-dimensional
ABS	Acrylonitrile butadiene styrene
PLA	Polylactic acid
SD	Standard deviation
HU	Hounsfield unit
TPU	Thermoplastic polyurethane
LAAO	Left atrial appendage occlusion (LAAO)
TEE	Transesophageal echocardiography
CTA	Computed tomography angiography
LCX	Left circumflex coronary artery
CAD	Computer-aided design
LAA	Left atrial appendage
PT	Patient
VR	Virtual reality
AR	Augmented reality

1. Introduction

1.1. Motivations

The traditional medical field has been dominated by standardized products and medical devices, which has been a hindrance to providing suitable medical treatment for patients with various diseases. Three-dimensional (3D) printing technology was first introduced to the medical field to overcome these limitations. With 3D printing technology, it is possible to produce various small quantities and there are no restrictions on the shape, which al-lows for the production of patient-disease-specific products. Using these features, it enables more precise medical treatment. 3D printing technology in the medical field is mostly based on medical images, and through secondary production, it has brought about a revolutionary change in the medical field. Recent research shows that the medical application of 3D printing technology is rapidly increasing both domestically and internationally. With 3D printing technology, it is possible to apply to various diseases and organs for preoperative simulation and produce customized orthopedic devices for patients with external deformities caused by various causes. Additionally, it also pro-vides an alternative for medical and health students for medical practice. Also, it is now possible to produce patient-disease-specific models, internal biomedical devices using biocompatible materials, and organ implants. The medical application of 3D printing technology is growing along with the development of 3D printing technology and materials, and medical technology is also evolving.

This study enabled surgical simulation by applying 3D printing technology to medical care for various purposes and reasons, manufacturing imaging phantoms based on medical images, and outputting human structures with different shapes according to individual patients as phantoms. In addition, a phantom for video thoracoscopic surgery simulation that can be applied to pediatric patients with less frequent and difficult surgery was created, and a phantom that can

educate and train residents and specialists was created and applied to clinical practice to evaluate its value.

1.2. Contribution

The main contributions of this study are summarized as follows. First, a study on the application of 3D printing using medical images was conducted. This can be applied to 3D printing using various medical images, and the medical 3D printing field will grow further along with the development of medical images. Second, the field of simulation phantoms can provide medical help to patients and medical doctors in surgical operations. In addition, it will be able to help with patient education and junior doctors' education. Third, the development of image phantoms for the evaluation of medical imaging software enables more accurate software management by reflecting the shape of abnormal lesions, which were difficult to evaluate with existing commercial phantoms.

This research will be of great help to the development and vitalization of medical 3D printing.

2. Backgrounds

2.1. 3D printing technology

3D printing technology has become increasingly prevalent in many fields due to the widespread distribution of various 3D printers and the development of materials. This technology is a process of layering materials to produce a three-dimensional shape using various printing methods. The different types of 3D printing technology are classified based on the properties of the material and the printing method.

One of the most commonly used 3D printing methods is Fused Deposition Modeling (FDM). This method uses heat to extrude filament material in the form of thermoplastic, building up one layer at a time. FDM technology is relatively affordable and is commonly used by beginners. However, due to its limitations, such as not being able to stack materials in the air, it generates a characteristic "supporter." Recently, it has been applied to various fields through changes in material diversity and printing methods.

Another 3D printing method is the PolyJet method, which is more expensive but offers high output stability and quality. This method mixes the inkjet and UV-curing methods, spraying materials from the fine nozzles of the printer head, which are cured by UV light simultaneously. PolyJet technology has the advantage of high output quality and the ability to adjust the color and hardness of the material.

The Digital Light Processing (DLP) method uses a projector to project a 2D image onto a photocurable resin, curing one layer at a time, resulting in fast printing speeds and high output quality. This method is advantageous in terms of high output quality and speed. Similarly, the first 3D printing technology, the Stereolithography (SLA) method, projects a laser beam onto a photocurable resin to create a shape and has the advantage of high output precision. However, the SLA method requires relatively expensive materials and careful control technology.

The ColorJet Printing (CJP) method uses an inkjet printer to spray liquid color ink and curing material onto powdered materials from the nozzle of the printer head to create a shape. Because the surface is formed using powder material, there is no need to generate a supporter, making surface treatment easy. In addition, since it uses CMYK ink, which is commonly used in inkjet printers, it is widely used in educational phantom production because it can reflect the desired color.

These are just some examples of the various forms of 3D printing technology and materials that can be selectively applied in the field of medicine. As 3D printing technology advances and becomes more accessible, the opportunities for its use in medicine are expected to continue to expand. From the production of medical implants and prosthetics to the creation of customized surgical tools and the development of innovative drug delivery systems, the possibilities are endless.

2.2. 3D printing in medicine

The application of 3D printing technology in the medical field has revolutionized the way medical products and devices are produced, enhancing precision, customization, and speed. One of the most significant contributions of 3D printing technology to the medical field is the production of medical artificial organs, medical parts, and dental implants. These products require customization based on the patient's anatomical characteristics and circumstances, and 3D printing technology can create them accurately and quickly.

Another area where 3D printing technology has found great utility in the medical field is medical education. Medical professionals can use 3D models to learn and gain experience in actual surgeries through simulation. This is particularly valuable in complex surgeries, where

a clear understanding of the anatomy is crucial to the success of the procedure. By providing an opportunity for medical professionals to gain hands-on experience in a risk-free environment, 3D printing technology can enhance the competence of medical professionals and reduce the possibility of malfunctions during surgeries.

However, it is essential to consider safety and efficacy when using 3D printing technology in the medical field. Product safety, performance, and quality must be certified, and biocompatibility must be verified when used with biomaterials. This is especially crucial in medical applications where patient safety is paramount. In addition, issues such as contamination and sterilization during the manufacturing process must also be taken into account to ensure the safety and quality of the final product.

As these challenges are overcome, it is expected that 3D printing technology will gain even more opportunities in the medical field. From the production of personalized medical devices to the creation of customized surgical tools and the development of innovative drug delivery systems, the potential for 3D printing technology to transform the medical field is enormous.

3. Case study

3.1. Imaging phantom: Chest computed tomography imaging phantom

3.1.1. Subjects

Quantitative computed tomography (CT) is becoming increasingly popular for diagnosing lung diseases and is being used to study a wide range of lung diseases. The recent outbreak of COVID-19 has led to a surge in research on lung diseases using CT images. However, it is important to ensure that the CT images are accurate and reliable for diagnosing and studying lung diseases.

One important aspect of ensuring the accuracy of CT images is the verification of intensity correction and quantitative measurement. To do this, we have developed CT imaging phantoms, which are physical models that mimic the structures and tissues found in the human body. These phantoms can be used to calibrate CT image intensity and validate the accuracy of quantitative measurement software.

Until now, developing CT chest imaging phantoms that accurately mimic the structures and tissues found in human lungs is challenging. While various types of CT imaging phantoms have been developed in the past, the development of CT chest imaging phantoms specific to patients and diseases has limitations.

Despite these limitations, many studies have focused on developing CT imaging phantoms to calibrate CT image intensity and validate the accuracy of quantitative measurement software. One such study aimed to fabricate a chest CT imaging phantom that reflects the CT intensity of various lung lesions using 3D-printing technology and silicone casting. The goal of this study was to evaluate the accuracy of the quantitative measurement obtained from the CT imaging phantom, which could help improve the reliability of quantitative chest CT for diagnosing and studying lung diseases.

3.1.2. Methods

To produce a CT imaging phantom using 3D printing, studies on Hounsfield unit (HU) values have used various silicone materials as 3D-printing materials. Materials research was conducted based on the shapes shown in HU and CT images of various materials. Various lesions were then extracted from the chest CT scans of the patients, and phantoms were manufactured using appropriate materials. HU evaluation was based on the well-known HU value of each anatomical structure of the human body. The measurement errors of the size between the reference and measured CT values of the inner diameter of the right ventricle, solid nodule, part of the lung vessel, and part of the airway were evaluated. The measured sizes were then analyzed using the Bland–Altman method. The overall workflow is shown in Figure 3-1-1.

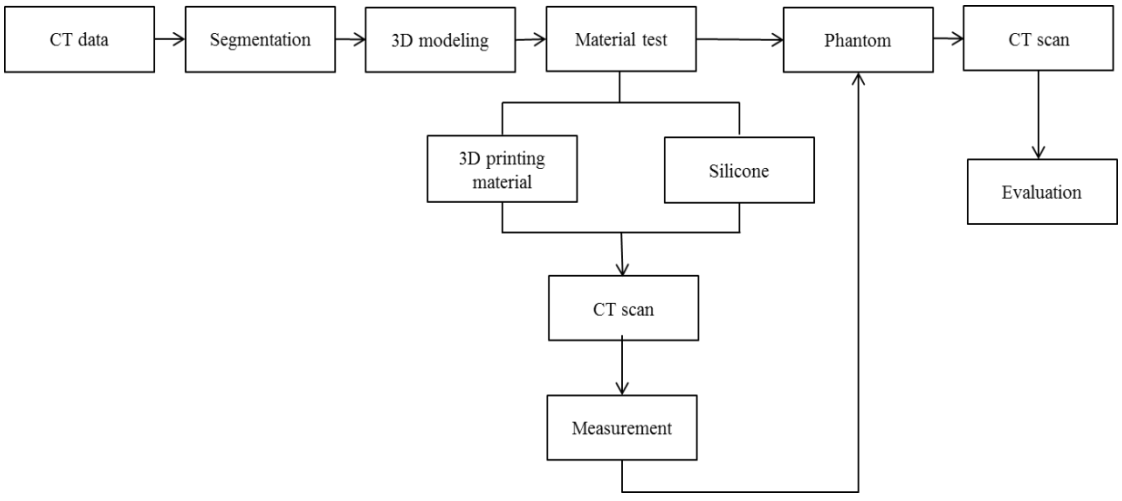

Figure 3-1-1. Overall workflow for fabricating a chest imaging phantom using three-dimensional printing and silicone casting.

Medical image acquisition

An anonymous patient, various silicone samples for fabricating phantoms, and 3D-printed chest phantoms were scanned using a dual-source CT (SOMATOM Definition Flash, Siemens

Healthcare) with a standard protocol of 120 kVp and 1.0 mm slice thickness. These scan data were also reconstructed to 0.6 mm in the axial section using software (Syngo CT 2012B).

Phantom design

The developed phantom reflects the human anatomy based on the chest CT images of a patient. The lung lobes, spine, ribs, heart, fat, and skin were designed (Figure 3-1-2). These anatomical structures were segmented using the medical image segmentation program Mimics software (Materialise Inc., Louvain, Belgium). For the design of the phantom model, a part of the chest CT section was modeled with 3-matic software (Materialise Inc.). Normal lung parenchyma and emphysema in the right lobe and solid nodule and fibrosis lesion in the left lobe were placed randomly. In addition, a thoracic cross-sectional model that included the heart, aorta, vertebrae, and ribs surrounding the lungs was made. Various anatomical structures were designed to be assembled on the lower plate in a negatively embossed manner. The skin, fats, and muscles were then made into separate layers to reflect the characteristics of each anatomy.

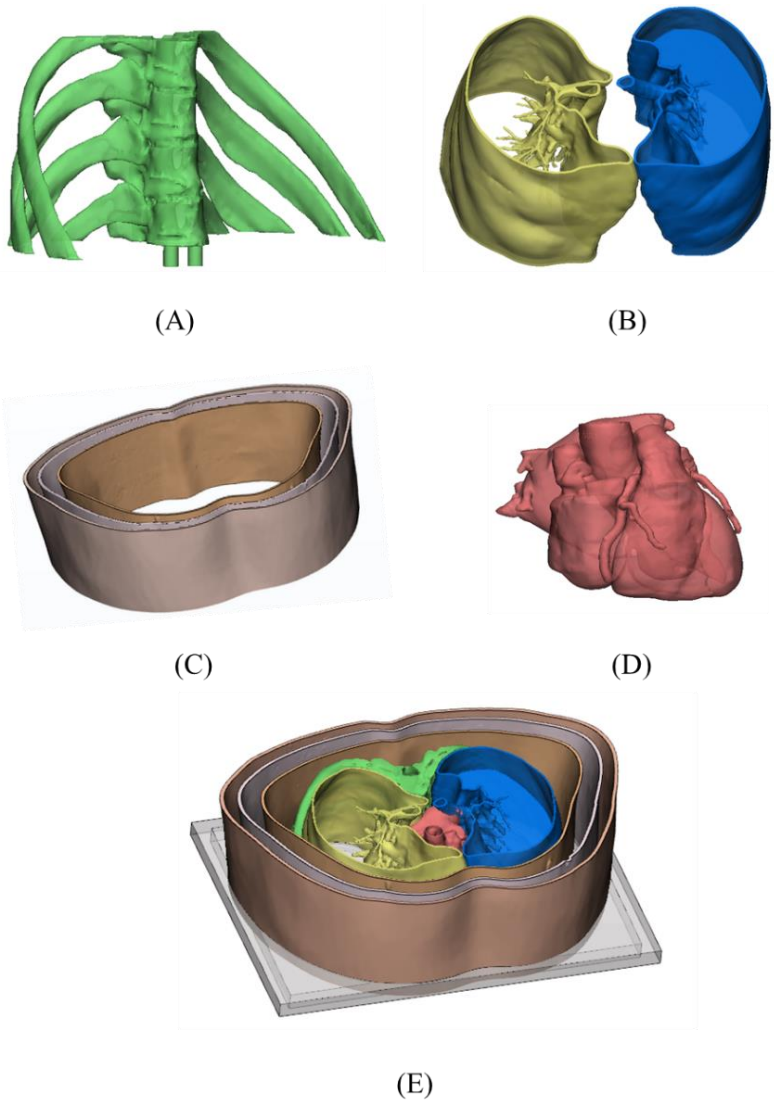

Figure 3-1-2. 3D modeling of chest CT image phantom based in CT images of a patient. (A) Spine and rib, (B) left and right lungs, (C) molder of the skin, fat, and muscle, (D) heart, and (E) composition of (A–D). CT, computed tomography; 3D, three-dimensional

3D-printing materials

The phantom molder was made using 3D-printing materials. The molder should be strong enough to avoid leakage of silicone, withstand the expansion force of silicone, and produce the chest CT axial phase of an actual adult. Therefore, robust and economical acrylonitrile butadiene styrene (ABS) material of fused deposition modeling (FDM) was selected and printed [21]. In addition, the heart model reflected the shape of a real heart using flexible thermoplastic polyurethane (TPU) material of FDM regardless of HU. The spine and rib were

printed using polylactic acid materials of hydrophilic FDM for HU implementation. Then, it was immersed in the contrast medium (Ultravist 370 mg I/mL; Bayer Healthcare, Berlin, Germany) for 48 h so that the printed material could absorb the contrast medium.

Silicone materials

First, to implement the pattern of the alveoli of the lung parenchyma in detail, CT was performed using some silicone materials to confirm its HU value. The silicone material was obtained from Smooth-On Co. of the FlexFoam-iT! series (Table 3-1-1). These silicone materials are expandable and durable. These can have an expansion rate from as high as 15 times to as low as 2 times. To ensure the reproducibility of the silicone work, a single researcher performed mixing using a silence mixing bar according to the specified ratios of silicone mixture, pot life, and hardening time. Therefore, the silicone to be used for the phantom was selected based on the CT intensity and pattern of each silicone. CT intensity was based on the HU for the human body [22,23], and the silicone pattern was selected by referring to the basic pattern corresponding to each lung lesion [24,25]. Therefore, to induce emphysema, the FlexFoam-iT! V was used in the lower right lobe of the lung, and to simulate normal lung parenchyma, FlexFoam-iT! 17 was used. In addition, to induce pulmonary fibrosis, FlexFoam-iT! 23FR was used, and the lung parenchyma containing solid nodule was tested with FlexFoam-iT! X.

Furthermore, to realize the fat and muscle surrounding the chest, gel wax and Ecoflex0020 silicone were used. Ecoflex 0020 silicone was used after mixing the main agent and curing agent in a 1:1 ratio, and air bubbles were removed using a deaerator. In addition, silicone of Dragon Skin FX Pro was used to model the skin.

Table 3-1-1. Summary of the silicone materials used for the chest imaging phantom

Material	**Ratio (main:hardner)**	**Pot life (23°C)**	**Hardening time (23°C)**	**Forming magnification**
FlexFoam-iT! X	1:1	60 (sec)	120 (min)	6 (times)
FlexFoam-iT! V	1:1	60 (sec)	120 (min)	11 (times)
FlexFoam-iT! 17	2:1	60 (sec)	120 (min)	3.5 (times)
FlexFoam-iT! 23	8.5:10	90 (sec)	120 (min)	2 (times)
Ecoflex 0020	1:1	1800 (sec)	240 (min)	−
Dragon skin pro fx	1:1	720 (sec)	40 (min)	−

Statistical evaluation

The CT value range was evaluated to compare the accuracy of the designed Standard Tessellation Language (STL) model and the measurements in the CT image of the 3D-printed phantom. All measurements were repeated five times each by one observer. For HU evaluation, the HU values of the normal lung parenchyma, lung diseases (fibrosis, solid nodule, and emphysema), and chest structures (muscle, fat, skin, and bone) were compared. To measure the shape accuracy, one part was selected from each anatomical region, and the length was measured using RadiAnt DICOM viewer (Medixant Inc., Poznan, Poland). STL images for 3D printing and CT images of the 3D-printed phantoms were measured (Figure 3-1-3).

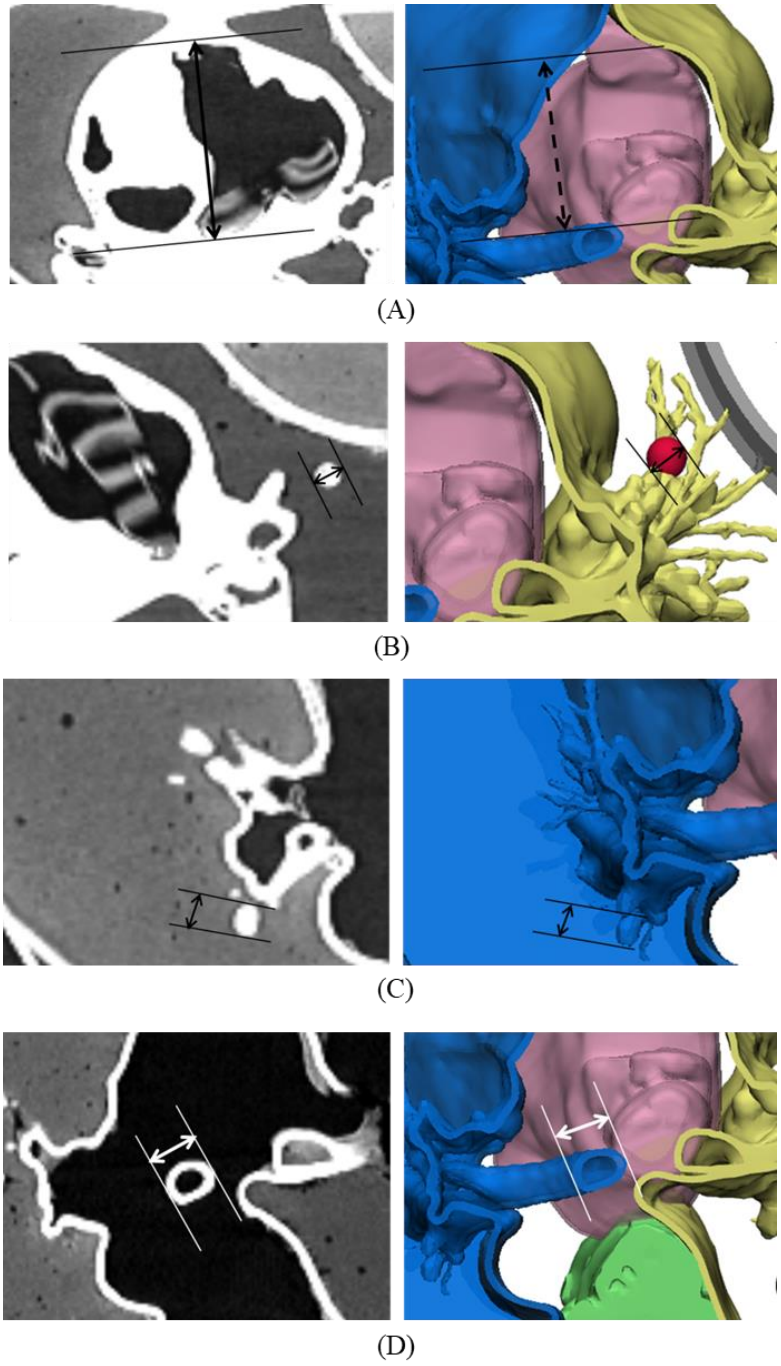

Figure 3-1-3. 3D-modeled and CT of 3D-printed phantom with landmarks specified for evaluating measurement error. (A) Inner diameter of the right ventricle, (B) solid nodule, (C) part of a lung vessel, and (D) outer diameter of the airway. CT, computed tomography; 3D, three-dimensional

3.1.3. Results

Baseline HU evaluation with different silicone materials

This study used a two-component silicone material that foams when the first and second agents are mixed. The degree of foaming varied with the type used, and as the silicone has different porosities, it was suitable for creating various patterns of lungs containing air. To realize the chest CT imaging phantom, various silicone patterns and HUs were identified. Silicone materials with various patterns and CT values were used to develop thoracic phantoms with various internal HU (Table 3-1-2).

Table 3-1-2. Lung structures matched with the HU of the FlexFoam-iT

Material	**HU**	**Lung structure**
FlexFoam-iT! X	−807.42 ± 5.71	Lung parenchyma with high HU
FlexFoam-iT! V	−885.82 ± 8.52	Emphysema
FlexFoam-iT! 17	−651.01 ± 15.97	Lung parenchyma with low HU
FlexFoam-iT! 23	−544.97 ± 13.63	Fibrosis

HU, Hounsfield unit

Chest imaging phantom for CT

Based on the aforementioned 3D printing and silicone casting, an axial section of the chest was taken from a CT image of a patient to produce a disease-specific chest imaging phantom. The lung lobes, heart, airways, muscle layers, fat layers, skin, ribs, and spine were modeled (Figure 3-1-4). In addition, various lung lesions were randomly constructed. The chest imaging phantom was made using various 3D-printing materials, patterns, and silicone materials. The HU values of the lung parenchyma, lung lesions, muscles, and fat layers as well as the morphology of the spine and ribs were realized in the CT image of the phantom. In addition, a shape similar to the axial phase of the human chest CT was modeled.

The human lung, which mainly contained air, had HU of −600 to −800 under normal conditions, < − 950 in the case of emphysema, −500 to −700 in pulmonary fibrosis, and −100 in solid nodules, and similar HU is implemented using various silicone materials. In an actual human body, the muscle and fat surrounding the lungs have 10–150 HU and −100, respectively, and the phantom also had similar values. Moreover, the phantom reflects the visual merit by

reflecting the hue and color of the external skin similar to the actual human body (Table 3-1-3 and Figure 3-1-4).

Table 3-1-3. Comparison of the HU values between the CT image and 3D-printed phantom [22,23]

		CT image value	Standard value	Phantom value
Normal lung parenchyma		-714.10±15.28	−600 to −800	−777.32 ± 24.84
Lung disease	**Fibrosis**	-	−500 to −700	−682.61 ± 22.92
	Solid nodule	-	~ −200	−41.86 ± 120.05
	Emphysema	-	−950 ~	−908.55 ± 18.32
Chest structure	**Muscle**	132.24±58.18	10 to 150	111.33 ± 23.22
	Fat	-70.24±22.79	−50 to −100	−159.60 ± 20.98
	Skin	85.72±15.38	−200 to +100	164.75 ± 28.92
	Bone	998.15±29.87	>1000	199.80 ± 24.14

(A) (B) (C)

Figure 3-1-4. Various CT image settings of the phantoms. (A) CT volume-rendering image of the phantom, (B) CT image of the phantom with lung window setting, and (C) CT image of the phantom with bone window setting. CT, computed tomography

The corresponding landmarks of the anatomical structures between the 3D-modeled STL and the CT image of printed phantoms were compared based on the measurements obtained and were evaluated using a Bland–Altman plot. The mean ± standard deviation of the differences was 0.20 ± 0.19 mm (limits of agreement, from − 0.1 to 0.5 mm) (Figure 3-1-5).

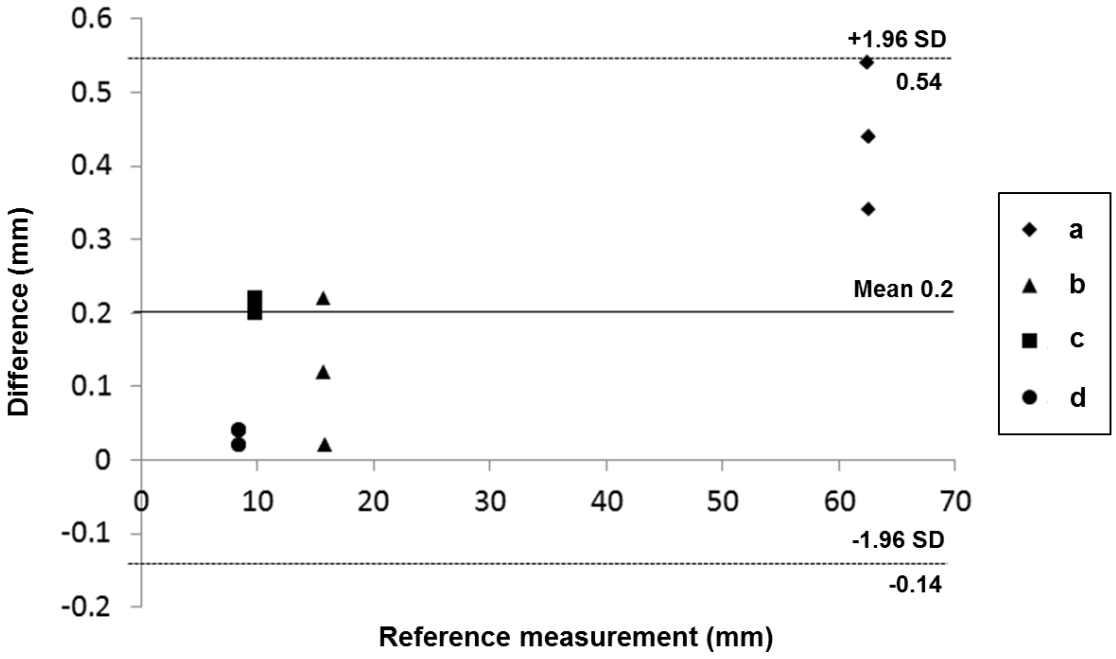

Figure 3-1-5. Bland–Altman analysis used to evaluate differences between the 3D-modeled STL (standard) and the CT from the printed phantom. (a) Inner diameter of the right ventricle, (b) solid nodule, (c) part of a lung vessel, and (d) part of the airway. CT, computed tomography; 3D, three-dimensional

3.2. Education phantom: Video thoracoscopic surgery simulation phantom study

3.2.1. Subjects

Advancements in surgical techniques and instrumentation, such as video-assisted thoracoscopic surgery (VATS), have significantly improved the ability of medical professionals to perform complex and delicate procedures in pediatric endoscopic surgery, including in small neonates[1,2]. However, despite these advancements, obtaining a comprehensive view of the operative field during these procedures still poses a challenge. In the clinical setting, one common application of thoracic surgery is the treatment of esophageal atresia with or without tracheoesophageal fistula (EATEF) in neonates. This condition is characterized by a gap in the esophagus that requires surgical repair to enable the infant to feed normally and can be especially challenging due to the small size of the neonate and the delicate nature of the esophagus[3,4]. Over the past 20 years, the number of minimally invasive surgical procedures in infants has significantly increased, including the repair of EATEF [3,5-7]. In 1995, the mean number of EATEF repairs performed by trainees in North America was 9.2 [8]. By 2006, the mean number of repairs for trainees dropped to 4.4 in the United States [9]. With few opportunities for trainees to perform EATEF repair, VATS for EATEF repair may not be effectively taught to an advanced level of proficiency within a short training period. In this way, VATS for infants is tricky for experts as well as novices.

Recently, 3D printing applications for reconstructing thoracic malformations in children have increased [1,2,10,11], requiring patient-specific products to meet medical needs, one of personalized medical product that has been pioneered. The 3D printing process for phantom fabrication has multiple steps: (1) acquisition of high-quality computed tomography (CT) data on the anatomical structure to be modeled, (2) image processing to extract the region of interest

from the anatomic structure, (3) 3D modeling from medical doctor needs, (4) quality assurance of the model to ensure its accuracy, (5) selection of the printing method and materials, and (6) printing of the phantom.

With these advances in medical 3D printing, a suitable phantom for VATS for EATEF training must be created using the medical image as well as to aid in the planning of complex surgical procedures [12-17]. However, it was limited to create the thoracoscopic simulator described various tissue properties with disease model; For that reason, most simulators have lacked certain details and realism until now [18-20]. Therefore, our study aims are three folds including 1) to fabricate a patient-specific simulator with measurement between stereolithography (STL) and simulators made by different 3D printers, 2) to fabricate realistic simulator with hardness measurement of various kinds of configurations, and 3) to fabricate a reusable thoracic simulator for VATS training in infant chest surgeries.

3.2.2. Methods

Medical imaging is required to produce patient-specific phantoms using 3D printing technology. Based on various medical images, such as CT and Magnetic Resonance Imaging (MRI), anatomical structures can be segmented and 3D modeled to create patient- or disease-specific 3D-printed models. Two types of 3D printers were used to fabricate actual phantoms with different materials. Shape accuracies and mechanical properties were evaluated to determine the final phantom, which was evaluated through simulation. The overall procedure is shown in Figure 3-2-1.

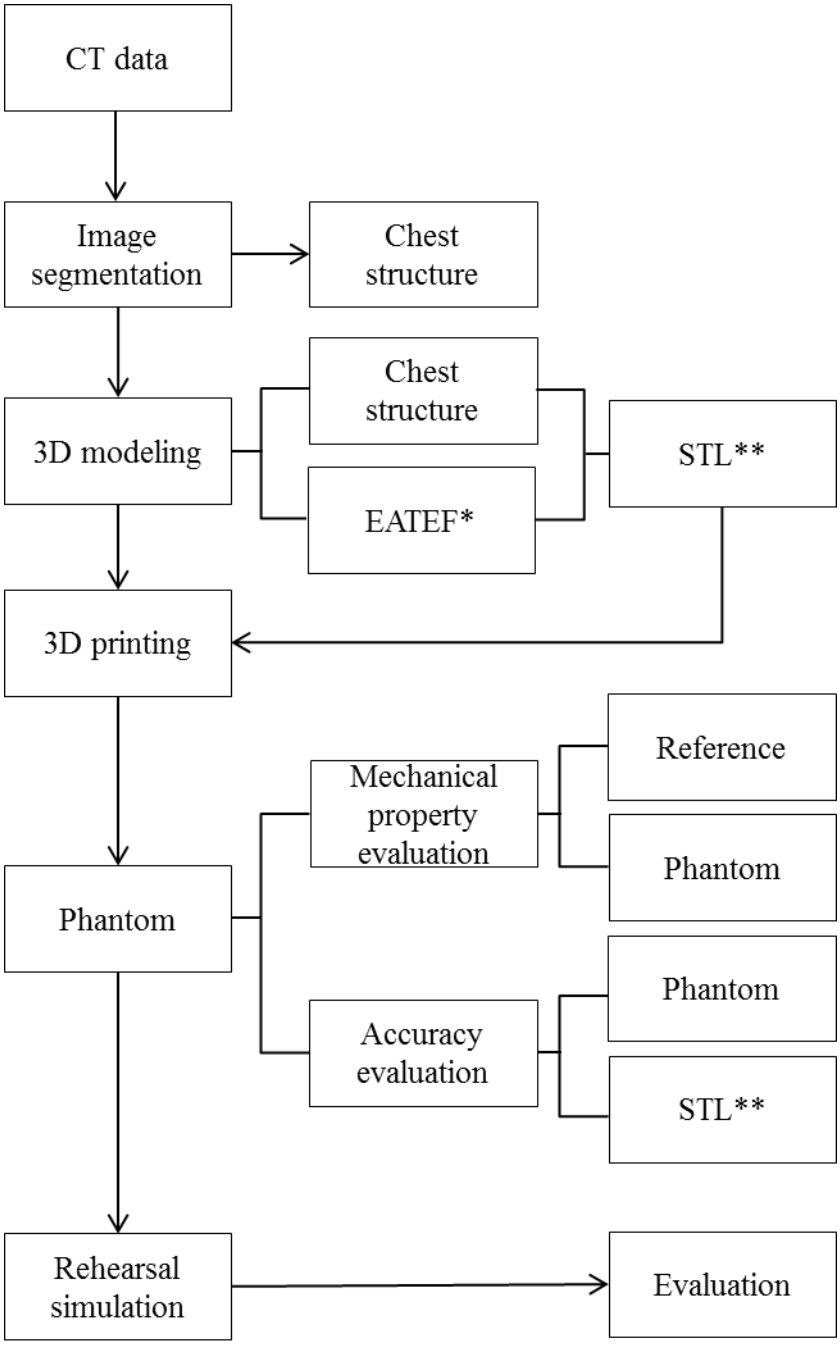

*EATEF: esophageal atresia with or without a trachea-esophageal fistula
** STL: stereolithography

Figure 3-2-1. Flowchart of the procedure for making 3D-printed infant VATS phantom.

Data acquisition

Contrast-enhanced lung perfusion CT images from a 3-year-old patient were used as the source of the 3D model. The application details of the scanning protocol are as follows: a SOMATOM Definition Flash CT scanner (Siemens Medical Solutions, Forcheim, Germany) was used with a rotation time of 0.37 s, a pitch of 1 with a feed of 21 mm per rotation, and a tube voltage of 80 kV, 85 mA. The in-plane resolution of the CT data is 0.4 mm, and the distance between slices is 0.6 mm. An acceptable thin slice resolution (<1 mm) is a key step because it has substantial effects on image resolution and noise, which in turn affect segmentation. The data includes the right lung tissue, esophagus, and structures within the thoracic wall, which are relatively less affected by motion artifacts of the heart.

3D modeling for simulation

The 3D models of the lung, esophagus, trachea, and chest wall, including bone, muscle, and skin, were generated using the software Mimics and 3-Matics (Materialise NV, Leuven, Belgium). Two-dimensional (2D) images were stacked by the software, yielding a threshold segmentation module with a set of tools, such as dilation, erosion, and boolean function, for the selection of pixels with gray values within a defined range of Hounsfield units representing the anatomical structures of interest. Subsequently, a region-growing algorithm was used to separate these structures of interest from the surrounding tissue. If the segmented anatomical structures were not clearly distinguished by a marked contrast in pixel gray values, then the desired pixels were manually drawn on each 2D CT image. 3D volume rendering models could also be refined by a volume-sculpting operation to achieve accurate representation of the desired organs in thoracic structures. Finally, the segmented 3D images were converted into

stereolithography (STL) format consisting of a triangular surface mesh structure by the software. The 2 mm wall thickness of the airway and esophagus was modeled by an outside offset function, and the fistula that was invisible in CT images was created using Meshmixer (Autodesk, Inc., Toronto, Canada). After that, seven artificial holes under each rib (third to eighth) were created for the placement of VATS ports. The scale of the model was reduced to 80% to match that of 9- to 12-month-old infants according to the Korean standard size. The diameter of VATS port holes was set to 12 mm by Magics RP (Materialise Inc., Leuven, Belgium). Finally, the unnecessary left half of the chest wall was cut out to reduce printing time and cost as well as for easy fixing onto the base panel.

To ensure the durability and efficiency of the simulator, it was divided into fixed and replaceable parts. The fixed part is the chest wall including the skin, muscle, bone structures, and esophagus model; the lung was separated as a replaceable part. The simulator was effectively applied to practice the various anatomical differences depending on the disease type (Figure 3-2-2).

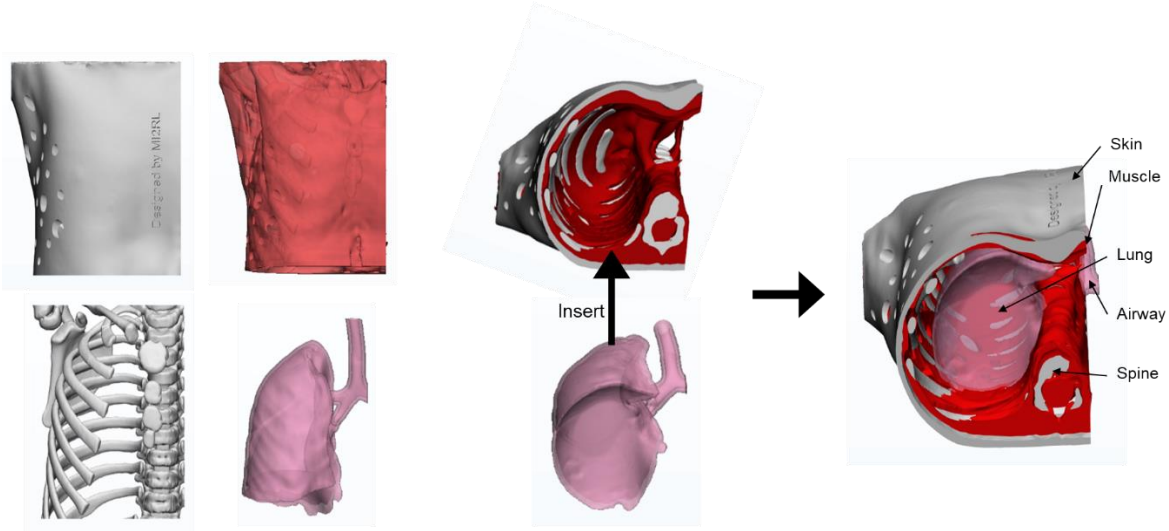

(A) **(B)**

Figure 3-2-2. 3D modeling for 3D rehearsal simulation phantom: (**A**) Right lung lobe, skin, muscle, bone, airway and lung (B) Detachable structure in which lung and airway structures can be replaced and inserted. (Mimics 20.0 and 3-matic 12.0, Materialise NV, Leuven, Belgium)

3D printing

The pediatric phantoms were produced using two types of 3D printers. For realistic simulation, holes of various sizes in the phantoms were implemented in the skin and muscle structure. Various types of airways with tracheoesophageal fistula were also designed and printed on reusable purpose.

Fused deposition modeling (FDM) 3D printer

The Good boT 6300MP printer (3D KOREA, CO, Korea) was used, which printed on KFLX28 filament. Conventional FDM 3D printers have difficultly printing on multicolored materials; however, the advantage of this printer is that it can print out various colors simultaneously. In particular, the KFLX28 filament used in simulator production had various colors and high flexibility and elasticity compared with existing acrylonitrile butadiene styrene (ABS) and polylactic acid (PLA). Using this feature, the lung, skin, muscle, bone, airway, and esophagus were printed on a replaceable structure. The skin and airways were designed specifically for the disease and patient and can be replaced.

PolyJet 3D printer

Using the Objet500 Connex3 printer (Stratasys, CO, USA), Vero color (hard material), and Aglius (soft material) can be effectively combined and printed immediately. In fact, the combination of PolyJet printing materials enabled the control of the elongation and hardness and reflected various elongation and hardness compared with FDM. Moreover, unlike FDM, colors and materials can be combined to generate structures of various hardness immediately. Therefore, the bones, muscles, and skin can be produced all at once, as well as produced separately to replace the lungs and airways.

Material properties

Using the refined 3D models and various materials, the thoracoscopic surgery simulator was produced using Good boT 6300MP and Objet 500 Connex 3. The two printers are often used for medical printing because the different colors of anatomical structures can be informative to clinical personnel.

The FDM 3D printer is highly commercialized and uses various types of materials, which are inexpensive compared with those of other types of printers. However, the hardness of these materials is difficult to control, and the surface is not smooth because the supporter is needed to overcome the inertia. PolyJet printers require more expensive materials and equipment compared with other printers, but the accuracy is high. In addition, the hardness can be adjusted by combining various types of materials with different elongations and hardness. This 3D printer offers the ability to print with dual materials to provide a wide range of soft, rubber-like models using Shore A hardness, elongation at break, tear resistance and tensile strength,

and rigid colored PolyJet photopolymers with multi materials from Vero color (hard material) and Aglius (soft material) (Table 3-2-1).

To implement the hardness of the anatomical structure, the elongation of each material was referenced (KFLX28 330 to 560%, Agilus and Vero 220 to 270%), and the hardness was directly measured. The KFLX28 material of the FDM fitting printer was measured for hardness by thickness, and the PolyJet type was measured by the material mixing ratio between Agilus and Vero.

Table 3-2-1. Comparison of two types of 3D printing: FDM and PolyJet.

	FDM	PolyJet
Cost	Low cost	High cost
Materials	Thermoplastic	Photopolymer
Feature	Multi-color, need to support	Multi-color, multi-material, soft, high accuracy

FDM = Fused deposition modeling

Accuracy evaluation

The phantom was printed by the two types of 3D printers from the same STL file. To compare the accuracy of each 3D-printed phantom with that of the STL modeling file, we assigned the same landmarks to four locations, which were measured by two researchers using Vernier calipers (Figure 3-2-3), for a total of eight measurements. Bland–Altman analysis was conducted to evaluate the STL file and 3D-printed phantoms using XLSTAT 2020 software. Paired t-test was used to compare the differences between the STL file and two types of phantoms using the SPSS software (trial version 25.00; IBM).

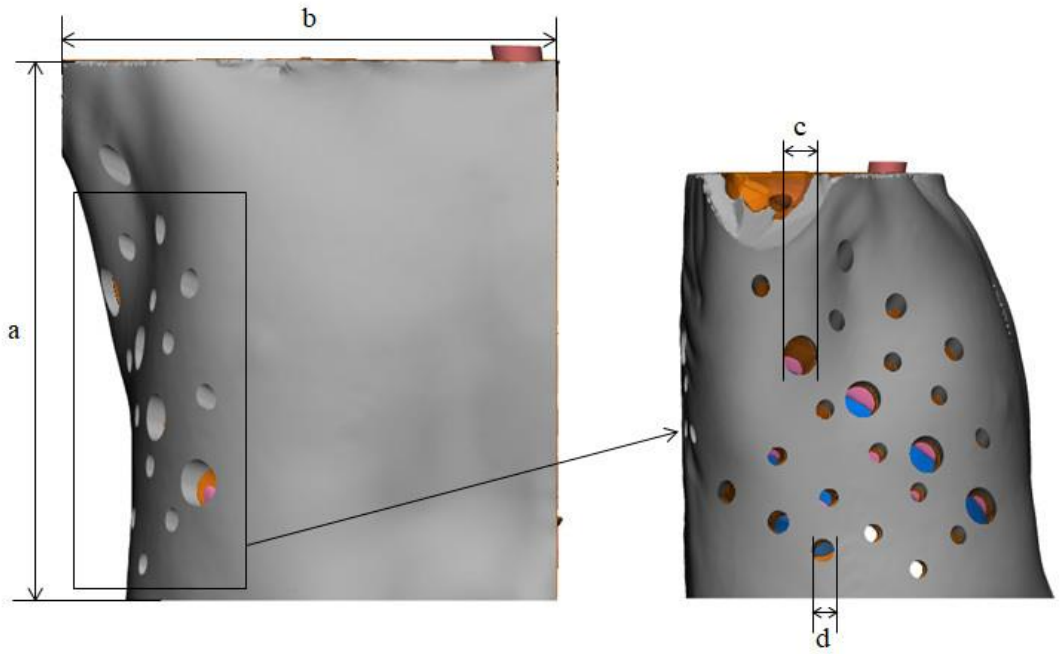

Figure 3-2-3. STL file with four landmarks specified for evaluating measurement error: (**a**) height, (**b**) width, (**c**) diameter of the VATS hole, and (**d**) diameter of another VATS hole. (3-matic 12.0, Materialise NV, Leuven, Belgium)

Simulation for VATS

A simulation was conducted for the VATS procedure of one infant with EATEF with this simulator and with conventional vendor provided simulator (Medtronics, MN, USA). One expert thoracic surgeon with over 15 years of experience evaluated the effectiveness of the 3D printed phantom in VATS for infant thoracic surgery. For the clinicians, the effectiveness of this simulator to conventional one was evaluated: (a) prediction of the effectiveness before using our phantom, (b) effectiveness after using our phantom comparing to the conventional one, and (c) the reality of the EATEF simulator was used.

3.2.3. Results

The 3D modeling process performed by an experienced operator consumed approximately 5–7 h (CT image to STL). Modeling and designing were the most challenging steps (3–4 h) owing to various issues, such as resolution, artifacts of CT images, and small anatomical structures (i.e., small size of the infant anatomy) in the CT images. The export of the reconstructed mesh surface to the STL file was simple and consumed only a few minutes. However, triangular mesh simplification with Meshlab 2020 (Visual Computing Lab, ISTI–CNR, Italy) and nonmanifold surface error fixing with Meshmixer consumed approximately 20 min.

Prior to implementation of the simulation phantom, the hardness of the materials used in the two printing methods was evaluated. The result shows that the materials could not be mixed in the FDM printing process and the hardness of materials differed according to the thickness of the printed object. At this time, the greater the thickness, the higher the hardness. In the case of PolyJet printing, the materials could be mixed. Therefore, the material mixture was printed and measured in 10 steps. The higher the proportion of Vero material (or the lower the proportion of Agilus material), the higher the hardness (Figure 3-2-4).

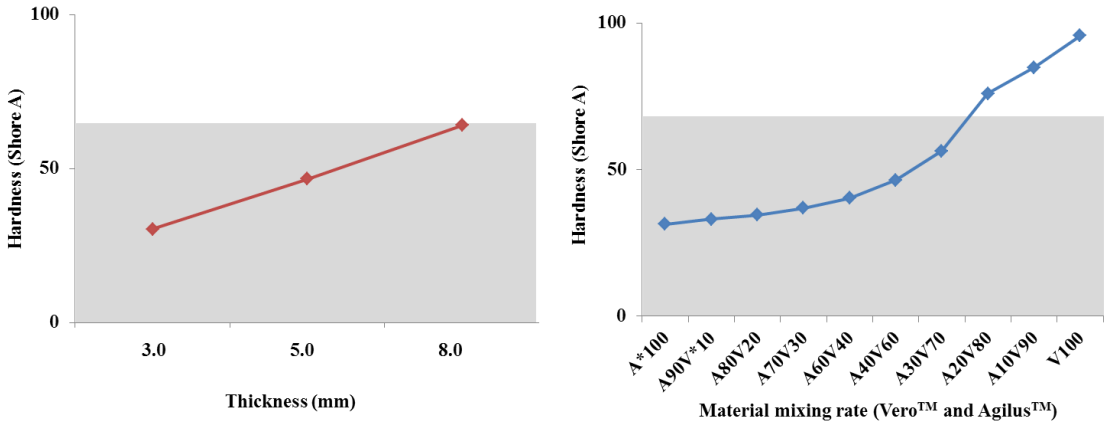

(A) **(B)**

Figure 3-2-4. Comparison of mechanical properties of 3D printing materials. The gray zone in both graphs is human skin to shore A hardness (mean) ranging from 0 to 65. (**A**) Hardness with different thickness values of FDM printing materials. (**B**) Hardness according to the mixing ratio of two PolyJet materials. (A*: Agilus, V*: Vero).

The corresponding metrics in the original STL file were compared with the physical measurements and evaluated using a Bland–Altman plot (Figure 3-2-5 and Table 3-2-2). In 3D printing with FDM, the mean ± standard deviation (SD) of the differences was 0.53 ± 0.46 mm (limits of agreement from −1.5 to 1.6 mm) (Figure 3-2-5A). In 3D printing with PolyJet, the mean ± SD was 0.98 ± 0.55 mm (limits of agreement from −2.3 to 2.4 mm) (Figure 3-2-5B). All of the measurements were within the limits of agreement.

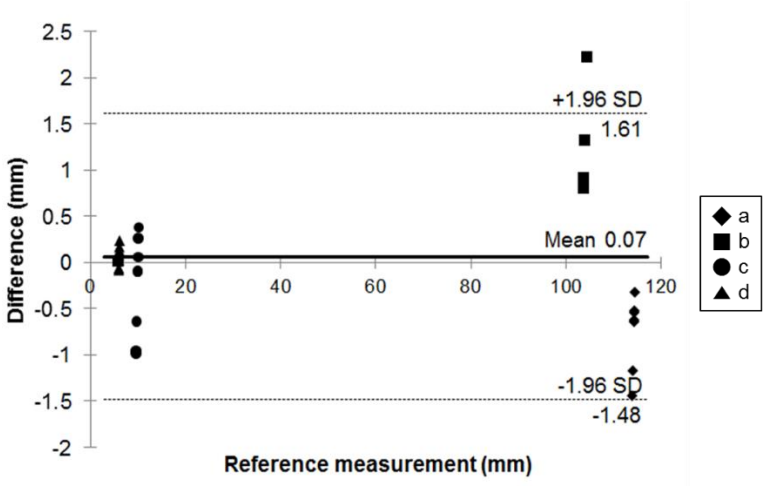

(**A**)

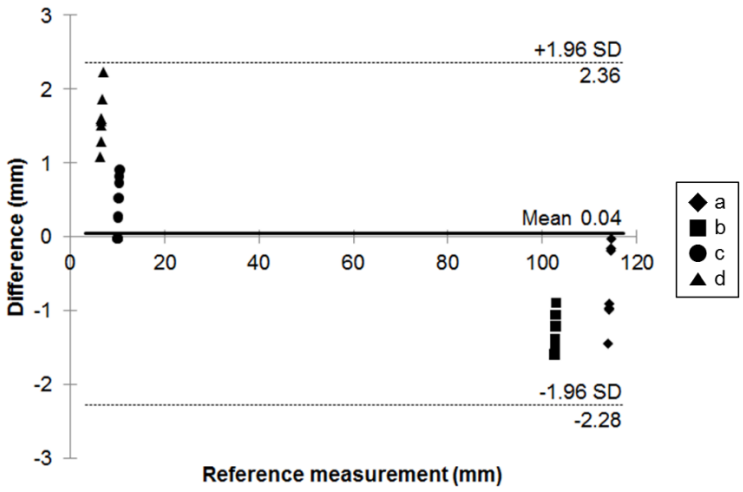

(**B**)

Figure 3-2-5. Bland–Altman analysis used to evaluate differences between the STL file (standard) and the two 3D-printed phantoms. (**A**) STL vs FDM, (**B**) STL vs PolyJet. The chosen landmarks were (**a**) height, (**b**) width, (**c**) diameter of VATS hole, and (**d**) diameter of another VATS hole in Figure 3-2-4.

Table 3-2-2. Comparison of FDM and PolyJet phantoms.

	FDM	PolyJet
Modality	Good boT 6300MP (3D KOREA, CO, Korea)	Objet500 Connex3 (Stratasys Ltd.)
Materials	KFLX28 filament	Vero, Agilus
Printing cost	$500	$1600
Printing time	72 h	16 h

FDM = Fused deposition modeling

Figure 3-2-6 shows that the infant thoracic phantoms fabricated by two types of 3D printing. With FDM, the anatomical structure was fabricated by assembly, and the hardness of the material was adjusted based on the thickness. In addition, unlike PolyJet printing, since there

is no transparent material, different colors were used to distinguish the anatomical structure. The phantom printed by the FDM printer consumed approximately 72 h, while the postprocessing consumed approximately 96 h. The 3D printing cost was $800. The PolyJet printer can control the hardness using material mixing. Therefore, various diseases can be reflected by replacing the airways and lungs. By mixing the materials, similar physical properties can be realized by reflecting various hardness values. The phantom printed by the PolyJet printer consumed approximately 16 h at a cost of approximately $1,600 (Table 3-2-3). The printing costs of each phantom were based on a quotation received from an outsourced company responsible for the final 3D printing. The cost includes materials used, time required, labor, and other factors, excluding processes such as image segmentation and 3D modeling to create STL files.

(**A**)

(**B**)

(**C**)

Figure 3-2-6. Pediatric thoracic phantom from 3D modeling and made with two types of 3D printers: (**A**) 3D modeling, (**B**) FDM, and (**C**) PolyJet. (3-matic 12.0, Materialise NV, Leuven, Belgium)

Table 3-2-3. Comparison of the reference measurements between the two types of 3D-printed phantoms.

Reference measurement – 3D-printed phantom	3D printing method	
	FDM	PolyJet
mean absolute difference (mm)	0.53 ± 0.50	0.98 ± 0.55
mean relative difference (%)	1.34 ± 0.85	8.15 ± 12.33

FDM = Fused deposition modeling

The simulator for VATS training was evaluated by an expert thoracic surgeon (Figure 3-2-7). The informed consent was obtained for identifying images 7(A) and 7(B) to publish the images. Based on the questionnaire, the surgeon responded as (a) prediction of the effectiveness before using our phantom, 3; (b) effectiveness after using our phantom comparing to the conventional one, 5; and (c) the reality of the EATEF simulator, 5. In addition, the surgeon commented that it is easy to plan the pre-operation and the time for surgery is reduced, and both types of phantoms were qualitatively rated as very useful in training and reflecting VATS than non-simulated before surgery. Especially, the texture of the anatomical structure could be realistically reflected by using the polyjet printing technology that can realize various hardness.

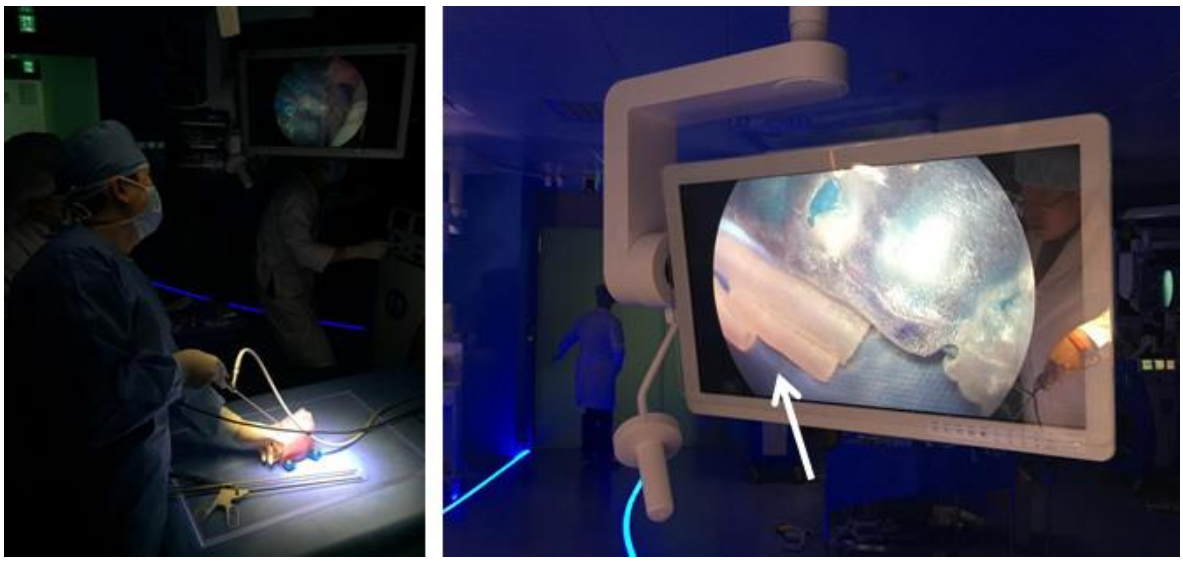

(**A**) (**B**)

Figure 3-2-7. VATS simulation with esophageal atresia with a tracheoesophageal fistula using 3D-printed phantom: (**A**) a surgeon's simulation of the 3D-printed phantom and (**B**) viewing the video screen (thick white arrow to indicate esophageal atresia with a tracheoesophageal fistula).

3.3. Rehearsal phantom: Left atrial appendage occlusion phantom study

3.3.1. Subjects

The left atrial appendage occlusion (LAAO) is a procedure that involves the use of occlusion devices to close the entrance of the left atrial appendage in order to block the source of thrombosis. This procedure is particularly relevant for patients with atrial fibrillation, as approximately 90% of thrombus is generated in the left atrium. Traditionally, anticoagulant medication has been used to prevent thrombosis and stroke in these patients. However, long-term use of anticoagulants can result in side effects such as bleeding, particularly in patients with old age or chronic illnesses. LAAO is therefore being proposed as a new therapeutic alternative to long-term anticoagulation.

Existing LAAO methods rely on 3D mapping and transesophageal echocardiography (TEE) or computed tomography (CT) angiography (CTA) to confirm the size and shape of the LAA and predict the device needed for the occlusion procedure. However, due to the various morphologies of the LAA, including cactus, chicken-wing, windsock, and cauliflower, leakage often occurs after the procedure.

The purpose of this study was to propose a patient-specific 3D printing technology that could be used for LAAO with CTA, and to evaluate the potential medical education value of this method. The proposed 3D printing technology would enable clinicians to create patient-specific models of the LAA, which could be used to practice and refine LAAO procedures before performing them on the actual patients. This could potentially reduce the risk of complications and improve the outcomes of LAAO procedures.

3.3.2. Methods

The process of creating patient-specific 3D-printed phantoms involves using medical images, such as CT and magnetic resonance imaging, to segment and model anatomical structures. This allows for the creation of a 3D model of the patient's anatomy that can then be printed using a 3D printer. In this study, two types of 3D printers were used to fabricate actual phantoms with different materials. The shape accuracy and mechanical properties of the printed phantoms were evaluated to determine the most suitable material for the final phantom. This material was then evaluated through simulation to ensure that it accurately represented the patient's anatomy. The stereolithography (SLA) 3D printer was used to fabricate the actual phantoms using resin materials. These phantoms were then used for a rehearsal simulation of LAAO procedures on 10 patients. The overall procedure is shown in Figure 3-3-1 of the study.

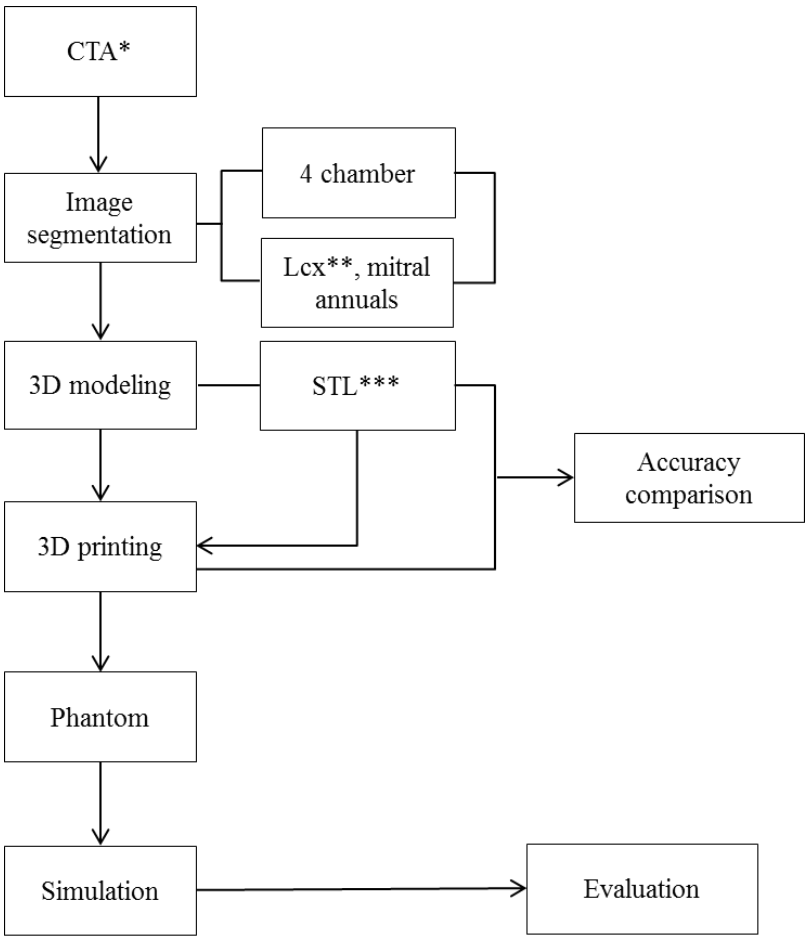

Figure 3-3-1. Overall workflow for developing rehearsal phantom for LAAO with 3D printing and CT image. 3D, three-dimensional; CTA, computed tomography angiography; LAAO, left atrial appendage occlusion; Lcx, left circumflex coronary artery; STL, stereolithography

3D-printing workflow

The procedure for fabricating 3D-printed rehearsal phantoms consists of multiple steps: (a) acquisition of a high-quality medical image of the anatomical structure, (b) medical image processing to extract the related regions of interest, (c) 3D modeling to accommodate the

unmet clinical needs, (d) quality check and determination of the accuracy of the 3D printed phantom, (e) selection of 3D printing type and materials, and (f) printing the phantom.

In order to make good use of the diversity of 3D printing technology, designing and planning to accommodate the unmet clinical needs is important. The material is different depending on the type of 3D printing technology, which lead to the different mechanical properties of the phantom. A summary of the features and material properties of both printing techniques is shown in Table 3-3-1.

Table 3-3-1. Descriptions of two types of 3D printing techniques, including FDM and SLA.

Printing type	Additive manufacturing process
FDM	FDM technology constructs objects layer-by-layer from the bottom up by heating and extruding thermoplastic filament. The process is somewhat similar to SLA, and specialized programs, or slicers, “cut” CAD models into layers and compute the manner in which the printer's extruder should assemble each layer.
SLA	SLA is a form of 3D printing technology used for producing models, prototypes, patterns, and creating parts layer by layer using photochemical processes by which light causes chemical monomers and oligomers to cross-link together to create polymers. This 3D printing type is quick and can make multi-designs; as such, it can be more expensive than FDM.

3D, three-dimensional; CAD, computer-aided design; FDM, fused deposition modeling; SLA, stereolithography

CT acquisition

The cardiac CTAs of patients with various diseases requiring LAAO were scanned with dual-layer spectral-detector CT (IQon Spectral CT ®, Philips Healthcare, Best, The Netherlands) according to the standard protocol of Seoul National University Bundang Hospital (Seongnam, Republic of Korea). The CT scans were acquired at 120 kVp with 0.67-mm slice thickness. In addition, images were reconstructed to 0.3-mm axial sections using image reconstruction

software (Spectral 3, Filter B, Philips, Best, The Netherlands). The data included the entire cardiac structure with the accompanying vessels.

Anatomical design

Modeling specific structures related LAAO is very important regarding the procedure, which is a vascular intervention, and a catheter is inserted into the patient's femoral vein to reach the left atrium. In particular, it is not open surgery; thus, it is important to determine the location of the LAA and its surrounding structures. The important structures for the LAAO rehearsal phantoms include the right atrium, left atrium, aorta, left superior pulmonary vein, LAA, left circumflex coronary artery, and mitral annulus (Figure 3-3-2). The four cardiac chambers, which have a relatively clear morphology, were easily segmented using the cardiac CT function of Mimics software. In contrast, the mitral annulus and left circumflex coronary artery, which do not exhibit clear shapes on the CT, were modeled by referring to the anatomical location.

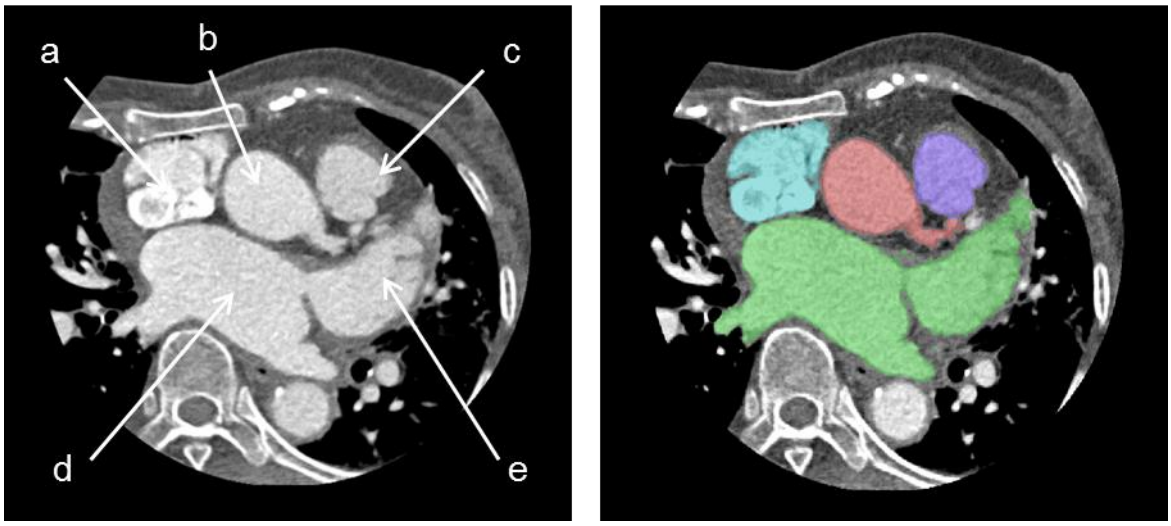

(A) (B)

Figure 3-3-2. Segmentation based on cardiac anatomy by cardiac CT angiography, including: (A) CT image based cardiac anatomy: (a) cavoatrial junction, (b) ascending aorta, (c) main pulmonary artery, (d) left atrium, (e) left atrial appendage; and (B) Segmentation based on CT angiography. CT, computed tomography

3D printing with different materials

The pilot study to determine 3D printing technology and materials was conducted to produce the rehearsal simulation phantoms. Thermoplastic polyurethane (TPU) material of fused deposition modeling (FDM) printer and flexible resin of SLA printer were printed with thicknesses of 0.8, 1.2, 1.6, and 2.0 mm. The size of the specimen was manufactured to be 3.0 × 3.0 mm, and, using a hardness tester, one researcher measured thrice for four locations to obtain an average value. As a result of measuring 95A shore hardness by thickness using the TPU material of the FDM printer, all of the specimens with a thickness of 0.8–2.0 mm were in the range of about 80–85 shore A. While measuring the hardness by thickness using the photopolymer resin of the SLA printer, the specimen with a thickness of 0.8–2.0 mm was in the range of 50–70 shore A. The result of the hardness measurement according to the ultraviolet (UV) curing time of the photopolymer resin was 54.6 shore A in 10 min. The hardness increased as UV was provided for more time. Although both materials were not within the range of actual human heart properties (which are less than 40), the 0.8-mm specimen, which is the smallest printable thickness of the SLA type, was the closest to the range of human heart properties (Figure 3-3-3).

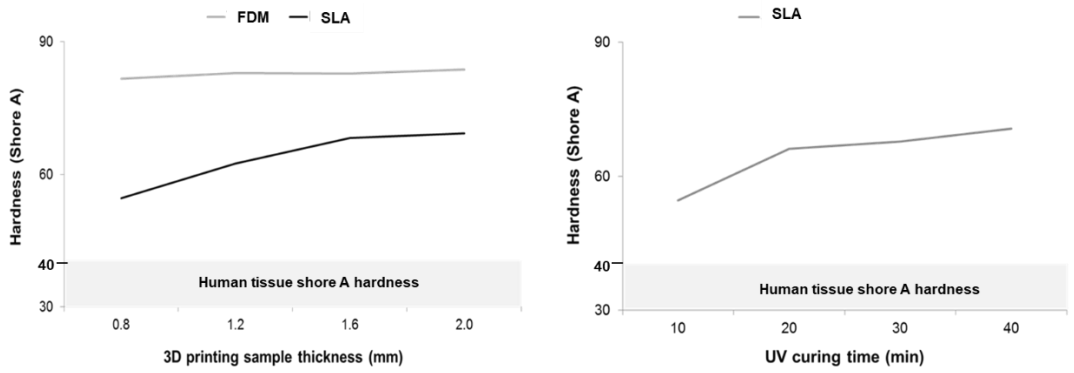

(A) (B)

Figure 3-3-3. Comparison of mechanical properties of 3D printing materials. The gray zone in both graphs is human cardiac tissue to shore A hardness (mean) of about 40. (A) Hardness with different thickness values of two FDM printing materials. (B) Hardness according to UV curing time of one material. 3D, three-dimensional; FDM, fused deposition modeling; UV, ultraviolet

The LAAO phantom was printed using both materials for the material test. One out of 10 patients enrolled in the study was randomly selected. For the patient, phantoms were printed using FDM and SLA 3D printers (Figure 3-3-4). Using the 3D-printed models with different materials, the LAAO rehearsal simulation phantoms were produced. The two printers are often used for medical printing due to their inexpensiveness and easy accessibility (Table 3-3-2). The FDM printer is highly commercialized and uses various types of materials, which are inexpensive compared with those used by other types of 3D printers. However, the hardness of these materials is difficult to control, and the surface is not smooth because the supporter is needed to overcome the inertia. On the other hand, SLA printers require more expensive materials compared with FDM printers, but the accuracy and surface smoothness are much

higher. In addition, the hardness and transparency of the printout can be adjusted according to the printout thickness and UV curing conditions of the SLA printer.

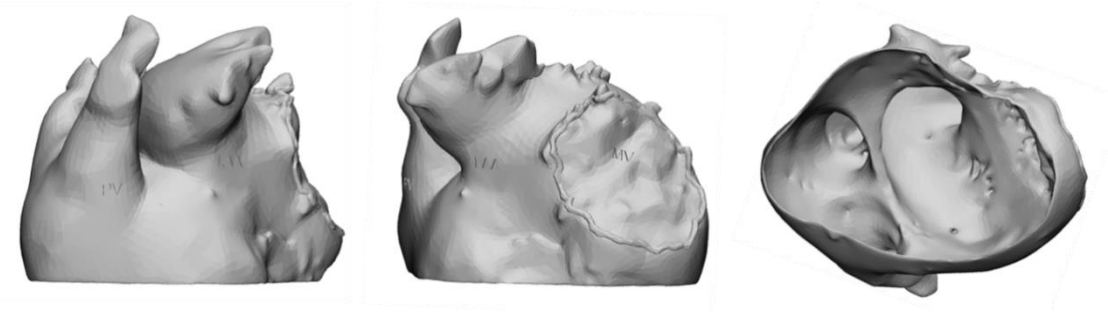

(A)

(B)

(C)

Figure 3-3-4. LAAO phantom made with two types of 3D printers. (A) 3D modeling (B) FDM, (C) SLA. 3D, three-dimensional; FDM, fused deposition modeling; LAAO, left atrial appendage occlusion; SLA, stereolithography

Table 3-3-2. Comparison of two types of 3D printing, including FDM and SLA.

	FDM	SLA
Cost	Low cost	Relatively high cost
Materials	Thermoplastic	Photopolymer
Feature	Opacity, multi-color, need to support	Transparency, soft, high accuracy

3D, three-dimensional; FDM, fused deposition modeling; SLA, Stereolithography

As an FDM printer, the Ultimaker S5 (Ultimaker BV, Geldermalsen, The Netherlands) was used with TPU 95A filament. Because the TPU 95A filament used in simulator production has a higher flexibility and elasticity compared with existing acrylonitrile butadiene styrene (ABS) and polylactic acid (PLA), TPU 95A was chosen among the various FDM filaments.

As an SLA printer, the X-Fab (DWS, Vicenza, Italy) was used with Flexa693, a photopolymer resin that has more flexibility and transparency. In addition, modifying the UV curing time of this SLA printer could control the elongation and hardness of the printout. Moreover, unlike FDM, the transparent material could be used for translucent printout.

Procedure for printing 3D rehearsal phantom

Figure 3-3-1 shows the overall procedure for printing the LAAO rehearsal phantoms. Materials for phantom production were selected through material property tests. The final phantoms of 10 patients were produced by the SLA printer with Flexa693.

The cardiac CTA images were segmented and modeled using the medical image processing softwares Mimics and 3-matics (Materialise, Leuven, Belgium). The segmentation results were confirmed by a radiologist and a cardiologist independently, each with more than 15 y of experience. This segmentation took less than 1 h by an operator (D.H.), not counting the time it took to update the segmentation as requested by a cardiologist.

Major anatomical structures related to LAAO were segmented and modeled for the phantom making. Each anatomical structure was segmented directly from patient-specific CT data. The modeled 3D images were converted into stereolithography (SLA) format, consisting of a triangular surface mesh structure, by the software. In addition, it was printed using the XFAB, the SLA 3D printer. Printing time varied from person to person, but most LAAO models took about 5 h to print. Post-processing took 1–2 h. This was because in the case of the SLA type, an isopropanol (purity grade >99.9%) cleaning process and an UV curing process were added to wash the resin after printing. Isopropanol washing took 15 min and UV curing took 10 min at 60°.

Accuracy comparison between the STL model and the 3D-printed phantoms

The 3D-printed phantom was printed based on the STL model. To compare the accuracy of each 3D-printed phantom with that of the STL model, the same landmarks of three different locations were measured by two observers. In addition, each observer measured each of them thrice, for a total of 180 times (Figure 3-3-5), using Vernier calipers. A Bland-Altman analysis was used to evaluate the accuracies between the STL model and printed phantom (Figure 3-3-6). Paired t-tests were performed to statistically compare the differences between the STL model and the 3D-printed phantom using the SPSS software (version 25.00; IBM Corp., Armonk, NY, USA).

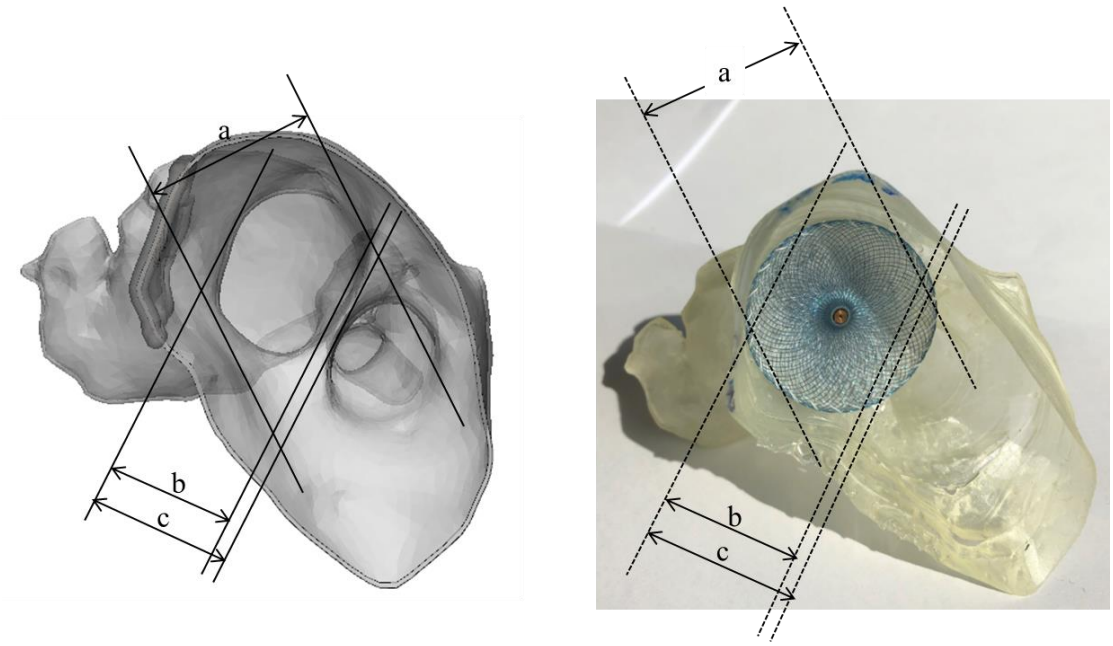

(A) (B)

Figure 3-3-5. Measurements of shape accuracy between 3D model and 3D-printed phantom. (A) The 3D model (STL) with three landmarks specified for evaluating measurement error. (B) The 3D-printed phantom with three landmarks specified for evaluating measurement error. (a, diameter of the horizontal zone; b, LAA ostium; c, vertical zone)

3D, three-dimensional; LAA, left atrial appendage; STL, stereolithography

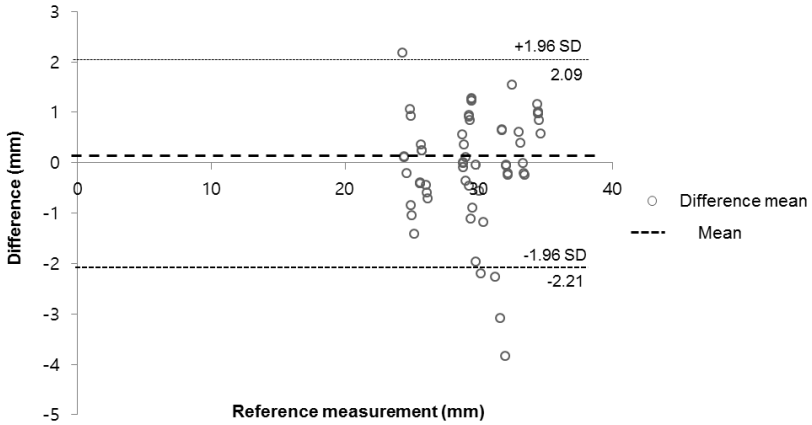
+1.96 SD
2.09
-1.96 SD
-2.21
Difference mean
Mean
Difference (mm)
Reference measurement (mm)

(A)

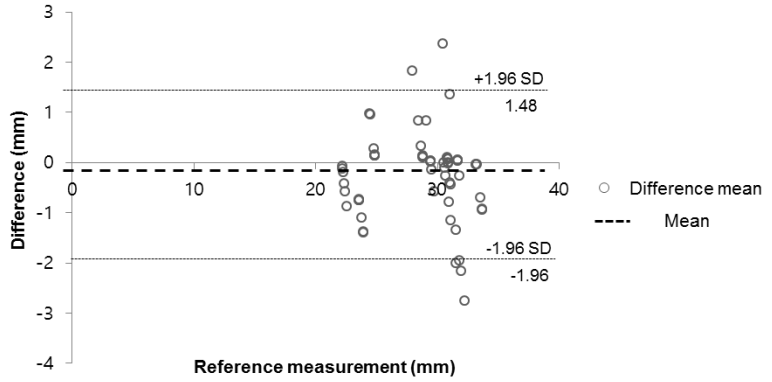
+1.96 SD
1.48
-1.96 SD
-1.96
Difference mean
Mean
Difference (mm)
Reference measurement (mm)

(B)

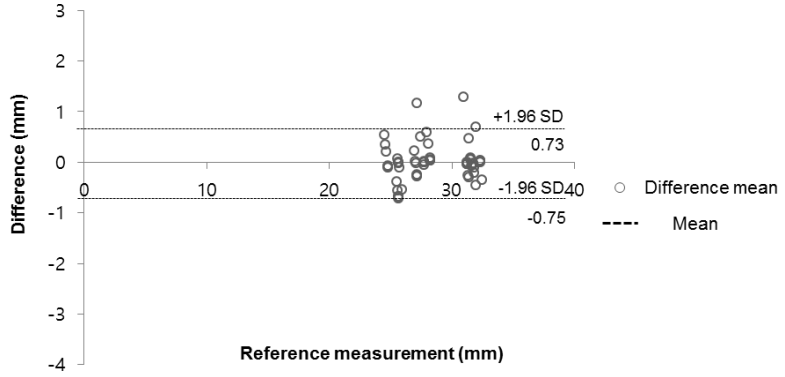
+1.96 SD
0.73
-1.96 SD
-0.75
Difference mean
Mean
Difference (mm)
Reference measurement (mm)

(C)

Figure 3-3-6. The Bland-Altman analysis to evaluate differences between the 3D model (STL) and the 3D-printed phantom. (A) Diameter of the horizontal zone, (B) LAA ostium, (C) Vertical zone. 3D, three-dimensional; STL, Stereolithography; LAA, left atrial appendage

Rehearsal simulation with 3D printed LAAO phantom

After producing the 3D-printed LAAO rehearsal phantom, a cardiologist simulated LAAO with the phantom. The clinician predicted the size of the LAAO device in the phantom simulation before the procedure and confirmed whether or not the size of the device used for the actual patient procedure was matched. In addition, the location and shape of the anatomical structures around the LAA were also confirmed (Figure 3-3-7).

(A) (B)

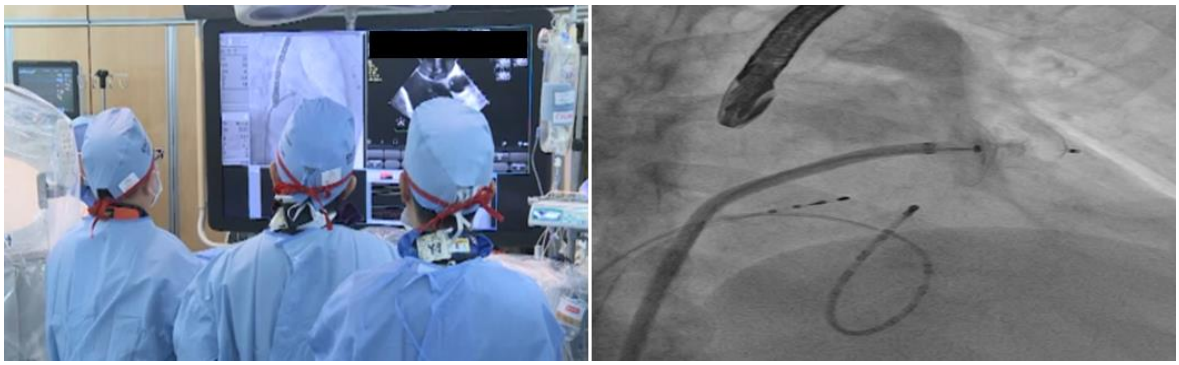

(C) (D)

Figure 3-3-7. LAAO was performed using a device of the predicted size. (A) A cardiologist performing TEE during the procedure. (B) Another cardiologist injecting saline, medicine, and medium contrast through the manifold. (C) Checking of fluoroscopy and TEE in real time during the procedure. (D) Confirmation of the device insertion predicted by fluoroscopy correctly into the LAA.

LAA, left atrial appendage; LAAO, left atrial appendage occlusion; TEE, transesophageal echocardiography

3.3.3. Results

The LAAO 3D segmentation and 3D modeling process from CT images to an STL model as performed by an experienced operator consumed approximately 1–2 h. The export of the reconstructed mesh surface to the STL file took just a few minutes. However, most of the time was spent in 3D printing and post-process. It took 1–2 d to print as thinly as possible. Therefore, it took at least 3 d for the overall procedure, from receiving the patient's images to finishing the phantom.

A pilot study to determine 3D printing technology and materials was conducted to produce the rehearsal simulation phantoms. As a result of measuring 95A shore hardness by thickness using the Vernier calipers. Consequentially, although the material itself is flexible, FDM using TPU is not suitable for rehearsing LAAO because the thermoplastic material does not stretch well. It was also difficult to check the location of the device due to its opaqueness.

The final phantom was produced using an SLA 3D printer as an LAAO simulation phantom. The material property of the phantom needs elasticity to withstand device expansion and

transparency to visually check the position of the device. Therefore, the LAAO rehearsal phantom was made using an SLA printer (X-Fab, DWS, Vicenza, Italy) with Flexa693, a photopolymer resin. Based on the material test results, the rehearsal phantom was printed with a thickness of 0.8 mm to maintain suitable physical properties through a 10-min UV curing process.

The corresponding landmarks between the original STL model and the printed phantoms were compared with the physical measurements and were evaluated using a Bland-Altman plot (Figure 3-3-6). As a result, the determined limits of agreement were from −1.8 to 1.6 mm (mean ± SD, 0.45 ± 0.37 mm). In addition, the greatest difference of the measured landmarks between the observers showed in the vertical zone. Among them, one patient showed a difference from the average value of up to 3.84 mm.

In addition, the rehearsal simulation for LAAO was evaluated by two expert cardiologists. The cardiologists predicted the LAAO device size for a total of 10 patients by using rehearsal simulation in consensus. In addition, the correctness of the predicted device sizes was evaluated by actual device sizes used in the actual procedure. The prediction accuracy for a total of 10 patients was 100%. The cardiologist performed LAAO using the predicted device. In addition, accurate 3D printing simulation was possible regardless of various LAA morphologies (Figure 3-3-7 and Table 3-3-3). Informed consent was obtained for the publication of identifying images 3-3-7(A-C).

Table 3-3-3. Rehearsal simulation results of 10 patients.

	Sex	3D printing simulation (mm)	Inserted device (mm)	Difference
Patient 1	M	34.0	34.0	0.0
Patient 2	M	28.0	28.0	0.0
Patient 3	F	25.0	25.0	0.0
Patient 4	F	28.0	28.0	0.0
Patient 5	M	31.0	31.0	0.0
Patient 6	M	25.0	25.0	0.0
Patient 7	M	34.0	34.0	0.0
Patient 8	F	34.0	34.0	0.0
Patient 9	M	28.0	28.0	0.0
Patient 10	F	25.0	25.0	0.0

PT, patient

4. Discussions

In this study, an imaging phantom with patient-specific and disease-specific characteristics was produced using medical imaging and 3D printing technology.

In this study, CT images were commonly used, and various 3D printing technologies were applied to the medical field. Therefore, there are differences in the purpose, material, and detailed technology of each study (Table 4-1).

Table 4-1. The comparison of 3 types of imaging phantom.

		VATS	Chest imaging phantom	LAAO
In common		Based CT image Used 3D printing technology		
Difference	Objective	Education and simulation	Software evaluation	Rehearsal simulation
	3DP technology	FDM, Polyjet	FDM, SLA	SLA
	3DP materials	TPE, Vero series and Agilus™	ABS, TPU, PLA	Flexi-693™
	Specific	Patient-specific	Disease-specific	Patient-specific

A variety of discussions are also needed in chest imaging phantom study. The existing commercialized CT imaging phantom is mainly used for the calibration of CT intensity, equipment maintenance, repair, and regular evaluation. Conventional phantoms also have some limitations, as they are not customized to each patient and disease, are expensive, and not realistic [30,31]. Therefore, our study focused on the fabrication of a patient- and disease-specific imaging phantom using 3D-printing technology that can overcome the limitations of conventional phantoms. The use of 3D-printing technology with various materials can simulate the CT intensity of various lesions, and the size, shape, and number of lesions can be realized. Therefore, 3D-printing technology makes it possible to easily manufacture patient-specific and disease-specific imaging phantoms. In the present study, CT chest phantoms were

developed to reflect various lung lesions with actual CT intensities and validate the accuracy of the quantitative measurements of the software. A molder for the chest phantom was made using ABS with 0–200 HU, and the spine and ribs were printed using hydrophilic polylactic acid (PLA), which is expected to absorb the contrast agent and has CT intensity like bones. In addition, the heart anatomy was printed using flexible TPU material so that it could be fixed into the chest phantom. By using silicone materials with foaming characteristics, various patterns of the normal parenchyma and lesions with actual CT intensity were made. The HU values of the normal lung parenchyma and emphysema, solid nodule, and fibrosis ranged from −800 to −600, -850 to −950, 100 to -200, and −500 to −700, respectively.

The strength of this study is attributed to the modeling of realistic lung lesions. The use of 3D-printing technology to create an imaging phantom helped overcome the limitations of existing commercialized phantoms. Many chest phantom studies have been conducted. Mei et al. demonstrated the feasibility of 3D-printed patient-based lung phantoms with accurate organ geometry, image texture, and attenuation profiles [32]. This study succeeded in realizing a part of a normal lung with CT intensity implemented using the pixel 3D-printing method. In addition, Hernandez-Giron et al. fabricated a 3D-printed anthropomorphic lung phantom for image quality assessment in CT, but its shape was very different from the patient anatomy [33]. In this study, the phantom evaluated the dose characteristics of the CT image, but the shape of the phantom was different from that of an actual human. Zhang et al. fabricated a personalized anthropomorphic phantom using 3D printing and tissue-compatible materials [34]. Craft and Howell prepared and fabricated a full-scale, sagittal-sliced, 3D-printed, patient-specific radiotherapy phantom [35]. However, these studies have some limitations in view of the realistic texture and shape of various lung lesions with actual CT intensity.

In this study, CT HU values of various lung lesions were represented using silicone materials. The FDM 3D printer is the most economical and accessible printing method, which could be one of its advantages for actual clinical applications. Developing a phantom with similar CT

intensity with an exact anatomical shape that represents the human body enables quantitative evaluation of CT software in realistic situations. It is also useful for educational purposes. With the CT image of the phantom that presents various lesions, the training efficiency of image reading for radiologists could be increased. In addition, a patient-specific model can help clinicians smoothly educate and communicate with patients about their diseases.

This study has several limitations. First, the CT intensity was not representative because the contrast medium was not absorbed well. In the future, the desired value will be reflected by mixing the appropriate amount of metallic FDM filament. Second, the shape of the heart was not accurate in the axial section of the chest CT image. To present the exact shape of the heart, additional research is needed to produce a similar image. Third, silicone was used by mixing and foaming the first and second agents. The ratio and pot life of the first and second agents may vary depending on individual mixing; thus, the porosity may change. In the future, this problem may be overcome through automation and mechanization of the silicone-mixing process. Fourth, the length measured between the 3D model and 3D-printed phantom CT image may differ depending on the thresholding value of the CT image [29]. Therefore, since the value can change depending on the boundary between the inner and outer surfaces of the same structure, reproducibility can be maintained by measuring the same image setting value of the CT image. In conclusion, using 3D-printing technology and silicone casting, we created a patient- and disease-specific chest imaging phantom that presents the CT intensity of lung lesions and shape of the actual human chest. In addition, various porous structures could be created using silicone castings to model lung lesions realistically. Unlike previous studies, a more realistic phantom was fabricated by reflecting various human structures on an axial section of the chest CT, which could be used for the evaluation of quantification software and CT intensity calibration.

In VATS study, most of the currently commercialized endoscopic surgical simulators are designed for abdominal surgery, and there are few types for thoracic surgery. Recently, with the introduction of VR, research for commercialization is in progress, but there is no VATS simulator for pediatric surgery except a general thoracic simulator. In particular, esophagus and trachea are small and special organs, and related simulators do not exist. In the case of pediatric, unlike adults, it is difficult to obtain an appropriate experience because the subject of minimally invasive surgery such as VATS is very rare due to their small size. Therefore, it could be meaningful that thoracic surgeons and pediatric surgeons can use the simulator to provide sufficient experience for minimally invasive surgery in pediatric. Moreover, because patients with EATEF are rare, determining whether efficient surgery is possible with VATS is not easy. The purpose of this study is to create a realistic simulator for a patient using 3D printing technology for VATS training in infant chest surgery. Therefore, to create a patient-specific phantom, we compared two 3D printing technologies and tried to devise a more realistic phantom. However, all the hardness suitable for human skin or tissue is difficult to determine. The properties of human skin and muscle are too variable to simulate and standardize. Several studies have shown that the mechanical properties of human skin depend on a variety of factors, such as age, gender, and location of the site [26-28]. Therefore, this study was conducted with reference to known mechanical properties of human anatomical features. The results of Blend–Altman analysis showed that the accuracies of both the phantoms and STL modeling files were acceptable for EATEF simulation in VATS. In general, it is known that PolyJet printing is much more accurate and expensive. However, in this study, some measurements using PolyJet have lower accuracy. In particular, the measured value of b (diameter of width) in Figure 3-3-5 is lower than that of the FDM phantom. Because the ratio of the Agilus material used for the skin and muscle was high and the soft material such as

Agilus of the PolyJet could not guarantee the shape accuracy [28], an error likely occurs in measurements using Vernier calipers. For the same reason, the measurement range of PolyJet is wider than that of FDM in d (diameter of vats hole) in Figure 3-3-5, which was made by combining Agilus with low-hardness PolyJet materials [29].

As several holes were marked on the skin to allow the port to provide various viewpoints of VATS endoscopies and anatomical variations of EATEF were replaceable, the phantom could be reused for various purposes in VATS. Even in cases requiring tumor or lung resection, such as tracheoesophageal fistula, mediastinal tumor, or lung tumor, if the internal model of the disease is generated, the thorax model itself can be recreated and simulated. However, for a more accurate procedure, a method of manufacturing a patient- and disease-specific simulator based on the medical image of the patient is available, which could be expensive. This phantom can also be used for various educational purposes, such as educating inexperienced junior surgeons or patients scheduled for surgery to provide them a better understanding of the disease and surgical procedures. The simulator has the potential to aid in pre-operative planning and serve as a surgical guide. The phantom for educational purposes can also be applied to augmented reality (AR) and VR as well as in simulation. Ten general thoracic surgeons used the simulator in this study. They (major, full-time, young professor) experienced VATS lung surgery on pigs in an animal lab as a beginner course. Then, as an advanced course, the VATS simulator for children of this study was used, and their feedback on this was delivered through discussion in the field. As a result, the difficulty of the procedure was very high, but everyone agreed that it was worth using it for rehearsal training in pediatric VATS surgery. Also, the evaluation of EATEF simulation by a surgeon with over 15 years of experience was positive, and the simulation of the 3D-printed phantom has a number of advantages over conventional surgery. By determining the complex anatomical variations

around EATEF in advance, difficult surgeries can be planned through rehearsal simulation, thus reducing the surgeons' effort, time, and burden. Moreover, this simulation can be extended to adult patients and for other procedures, such as VATS lobectomy. This type of preoperative experience will enable surgeons to perform thoracoscopic surgery efficiently and safely and improve surgical outcomes by allowing them to recognize the critical surrounding structures.

This study has several limitations. First, simulation was performed by only one surgeon who reviewed the materials and clinical acceptability of the phantom. Since our paper focused on development of a simulator, this procedure was very difficult and the number of operations was not large, it was not possible to gather opinions from various surgeons. Therefore, we cannot assume that these findings will be reproduced by all surgeons. More surgical cases and more surgeons' opinions will be collected in further studies. In addition, given that this study was based on the CT image of only one pediatric patient, there is a limit to reflecting the diversity of the anatomical abnormalities of EATEF, and it can be applied only in the training of thoracic surgeons specializing in pediatrics. In the future, phantoms of many patients should be fabricated and evaluated by multiple surgeons. If simulation is required for surgeons of various experiences, various conclusions can be drawn. By supplementing the size or internal anatomy, the simulation phantom training could be supplementing the size or internal anatomy, the simulation phantom training could be extended to various kinds of thoracoscopic phantoms that reflect the age, sex, and specific diseases of both children and adults. At present, available 3D printing materials are not completely satisfactory and are different from the human thoracic portion in terms of their mechanical properties, including hardness, and elasticity. Thus, to produce more realistic simulators, research must be conducted by developing and combining silicone casting and various 3D printing materials.

In the LAAO study, that is a structural intervention performed by checking certain regions, based on the medical image, during the procedure. TEE performed in the LAAO procedure makes image acquisition easy and fast, but it is difficult to accurately measure the 3D form and understand the shape. The lobe diameter measured by CT and TEE is measured assuming that the LAA is a cylinder. However, since the lobe has a thickness of 7.5 to 10 mm, there is a difference between the proximal landing and distal landing zone diameters when the lobe is inserted the LAA. In addition, because the cross-section of LAA is elliptical rather than circular, there can be long and short diameters in one plane. However, this depends on the plane being measured; thus, it could differ from the real one. To minimize these problems, the rehearsal with the 3D printing phantom before the procedure was evaluated while the device was inserted. In this way, the shape of the device after insertion (shape-stable, hockey puck-unstable/undersized, or strawberry-unstable/oversized) could be evaluated, and the stability of the device position after insertion could be assessed through a tug test to actually check the line of the device axis and the LAA neck axis. In addition, the position of the left circumflex artery (LCx) can be evaluated, and the relationship between the lobe and the LCx could be confirmed after the actual insertion. The actual structure can be judged in terms of whether the final device covers the appendageal ridge well or whether it does not invade the mitral valve. However, due to the limited number of cases, further research is needed to derive objective results. Also, the application of 3D printing technology requires more cost and time, so it should be considered and applied reasonably.

Flexible and transparent materials were selected in order to simulate the phantom with materials having properties similar to those of human tissue, considering the reasonable cost for manufacturing patient-specific phantoms. TPU of FDM 3D printer is a polymer-based material with some flexibility. Compared to SLA materials, this is not as flexible and

transparent, so it could not be applied to actual rehearsals. Therefore, in this study, we used the flexible material of SLA has relatively good elasticity and transparency enough to see the positioning of the LAAO device from the outside, which could be a novelty of our method. In addition, the implementation of the physical properties of the actual human anatomical structure was attempted in order to show that the handling of the procedure can be similar. The material was decided upon by collecting the opinions of two cardiologists, referring to the shore A hardness of 3D printing materials with a texture similar to that handled in the actual treatment. Although it is difficult to apply this study to actual clinical practice right now due to costs or healthcare reimbursement, this method with 3D printing technology could have a potential to supplement current medical cares like an educational simulator for medical students and intervention fields with high image dependence.

This study had several limitations. First, only two medical doctors evaluated the suitability of the materials. In addition, despite an estimated 3-y study, the number of LAAOs was not sufficiently large, with only 10 patients enrolled. Therefore, there is a need to evaluate this phantom with more anatomical diversity of various kinds of LAAO patients in future studies. It should also be evaluated by the various cardiologists and by collecting various opinions through questionnaires. Second, it was difficult to accurately implement the texture of the actual human body with the currently available 3D printing materials. Therefore, to reflect physical properties more similar to that of the actual human body, it is necessary to develop silicon and similar 3D printing materials. Third, there was a limitation in the measurements performed for comparing the accuracy between the STL file and the 3D-printed phantom. There were outliers where a value outside the 95% confidence range appeared, as shown in Figure 3-3-6. To make it similar to the physical properties of the actual heart tissue, it was manufactured to be as thin and flexible as possible; thus, the measurement value may not be

constant, depending on the operator who uses the Vernier caliper when measuring. In particular, the landmark C in Figure 3-3-5 is a measurement of the vertical area of the orifice, which was very difficult to measure using Vernier calipers due to the shape of the area and the material characteristics of the phantom. However, in the actual procedure, the accuracy of the device size prediction of the 3D printing phantom was very high because a circular device that filled in the LAA orifice was inserted. Fifth, the size of the LAA in the CT image may not have been fully reflected in some cases, depending on the patient's condition at the time of the CT scan. Therefore, CT scans prior to the procedure should be performed with caution. Therefore, this rehearsal simulation using a 3D-printed LAAO phantom more accurate device size selection is possible because the 3D shape and architecture can be evaluated using the 3D-printed phantom, compared to the conventional method that predicted the device size using only CT and TEE. In addition, there may be a dependency on the researcher who manually performs image segmentation and modeling when segmenting individual patients' CT images. This can be overcome through the automation of medical image segmentation and 3D modeling.

5. Conclusions

3D printing is one of the strategic technologies leading technological innovation worldwide, gradually changing the culture of the medical field and expanding its application area. Furthermore, medical 3D printing is advancing with greater synergy by incorporating autoCAD and AR/VR technologies, alongside the utilization of artificial intelligence.

This paper studied the application technology and development of the medical field incorporating 3D printing technology. 3D printing is designed using various medical images and produced by layering materials. This makes it possible to manufacture related devices in the medical field that cannot be designed and manufactured with existing technologies, which enables manufacturing innovation in the medical industry. Medical 3D printing technology enables rapid prototype development and evolves the supply chain.

In this study, a medical image-based phantom can be produced with a 3D printer and used for simulation to prevent medical accidents, reduce surgical time, improve the success rate of surgery, and train medical staff. In addition, by developing a phantom that reflects lesion simulation and body-specific features for a software evaluation, software evaluation can be applied to various lesions that were previously impossible. As such, medical 3D printing can enable innovative product development and increase clinical efficacy, resulting in ultimate benefits to patients and the medical field.

Abstract (In Korean)

의료 3D 프린팅은 복잡한 수술 및 의료 절차에 맞춤형 솔루션을 제공함으로써 의료분야에 혁신을 가져올 수 있다. CT 및 MRI 등의 이미징기술을 이용하여 3D 프린팅은 매우 정확하고 사실적인 환자 해부학 모델을 생성할 수 있고, 이를 통해서 수술을 계획하고 리허설 시뮬레이션을 가능하게 한다. 또한 개별환자의 요구에 맞는 의료기기를 생산할 수 있다. 특히, 의료분야에서 3D 프린팅의 이점 중 하나는 환자, 질환 맞춤형 등 사실적인 형상 및 환자별로 재사용가능한 팬텀을 제작할 수 있다는 것이다. 이는 발생 빈도가 적은 비교적 어려운 수술에 있어서 외과의가 실제 수술을 수행하기전 리허설을 가능하게 하고, 이를 통해 환자에게는 더 나은 결과를, 외과의에게는 더 높은 완성도의 수술을 가능하게 한다. 또한 기존 기술로는 불가능했던 다양한 병변이 반영된 팬텀을 이용하여 의료영상 소프트웨어 평가를 수행함으로써 의료영상의 퀄리티를 높이고 의료영상장비의 정도관리에 적용할 수 있다. 본 연구에서는 의료영상, 3D 프린팅 기술과 발포실리콘을 이용하여 다양한 HU 를 구현하고 질병의 패턴을 반영한 흉부팬텀을 제작하여 정량화 소프트웨어 평가에 적용할 수 있었다. 또한, CT 영상 기반 소아 비디오 흉강경 시뮬레이션 팬텀의 제작은 난이도가 높고 빈도가 적은 소아 침습 수술에서 환자와 외과의에게 시술 전 리허설 시뮬레이션을 통해 수술의 정확도를 향상시키고, 시술시간을 단축시키는 등의 효과를 도출할 수 있었다. 마지막으로 좌심방이 폐색술 리허설 시뮬레이션 팬텀은 시술 전 시뮬레이션을 통해 삽입 장치의 사이즈 예측 및 주변 해부학 구조물과의 관계를 미리 파악하고 보다 정확한 시술을 가능하게 하였다.

결론적으로, 의료영상과 3D 프린팅 기술은 고도의 맞춤화 기술을 실현하고, 혁신적인 의료기술에 대한 새로운 가능성을 보이고 있으며, 기존 의료의 공정을 3D 프린팅 기술로서 향상시키고 개선하여 높은 수준의 의료를 가능하게 한다.

6. Reference

1. Burke RP, Wernovsky G, van der Velde M, Hansen D, Castaneda AR. Video-assisted thoracoscopic surgery for congenital heart disease. *The Journal of thoracic and cardiovascular surgery.* 1995;109(3):499-508.
2. Cano I, Antón-Pacheco JL, García A, Rothenberg S. Video-assisted thoracoscopic lobectomy in infants. *European journal of cardio-thoracic surgery.* 2006;29(6):997-1000.
3. Gonzalez D, Paradela M, Garcia J, dela Torre M. Single-port video-assisted thoracoscopic lobectomy. *Interactive cardiovascular and thoracic surgery.* 2011;12(3):514-515.
4. Jensen K, Bjerrum F, Hansen HJ, Petersen RH, Pedersen JH, Konge L. Using virtual reality simulation to assess competence in video-assisted thoracoscopic surgery (VATS) lobectomy. *Surgical endoscopy.* 2017;31(6):2520-2528.
5. Burjonrappa S, Youssef S, St-Vil D. What is the incidence of Barrett's and gastric metaplasia in esophageal atresia/tracheoesophageal fistula (EA/TEF) patients? *European Journal of Pediatric Surgery.* 2011;21(01):25-29.
6. Holder TM, Cloud DT, Lewis JE, Pilling GP. Esophageal atresia and tracheoesophageal fistula: A survey of its members by the Surgical Section of the American Academy of Pediatrics. *Pediatrics.* 1964;34(4):542-549.
7. Little DC, Rescorla F, Grosfeld J, West K, Scherer L, Engum S. Long-term analysis of children with esophageal atresia and tracheoesophageal fistula. *Journal of pediatric surgery.* 2003;38(6):852-856.

8. Rowe MI, Courcoulas A, Reblock K. An analysis of the operative experience of North American pediatric surgical training programs and residents. *Journal of pediatric surgery.* 1997;32(2):184-191.

9. Sømme S, Bronsert M, Kempe A, Morrato E, Ziegler M. Alignment of training curriculum and surgical practice: implications for competency, manpower, and practice modeling. *European Journal of Pediatric Surgery.* 2012;22(01):074-079.

10. de Lagausie P, Bonnard A, Berrebi D, Petit P, Dorgeret S, Guys JM. Video-assisted thoracoscopic surgery for pulmonary sequestration in children. *The Annals of thoracic surgery.* 2005;80(4):1266-1269.

11. Koontz CS, Oliva V, Gow KW, Wulkan ML. Video-assisted thoracoscopic surgical excision of cystic lung disease in children. *Journal of pediatric surgery.* 2005;40(5):835-837.

12. Mowry SE, Jammal H, Myer IV C, Solares CA, Weinberger P. A novel temporal bone simulation model using 3D printing techniques. *Otology & Neurotology.* 2015;36(9):1562-1565.

13. Chae MP, Rozen WM, McMenamin PG, Findlay MW, Spychal RT, Hunter-Smith DJ. Emerging applications of bedside 3D printing in plastic surgery. *Frontiers in surgery.* 2015;2:25.

14. Weinstock P, Prabhu SP, Flynn K, Orbach DB, Smith E. Optimizing cerebrovascular surgical and endovascular procedures in children via personalized 3D printing. *Journal of Neurosurgery: Pediatrics.* 2015;16(5):584-589.

15. Barber SR, Kozin ED, Dedmon M, et al. 3D-printed pediatric endoscopic ear surgery simulator for surgical training. *International journal of pediatric otorhinolaryngology.* 2016;90:113-118.

16. Tai BL, Rooney D, Stephenson F, et al. Development of a 3D-printed external ventricular drain placement simulator. *Journal of neurosurgery.* 2015;123(4):1070-1076.

17. Parthasarathy J. 3D modeling, custom implants and its future perspectives in craniofacial surgery. *Annals of maxillofacial surgery.* 2014;4(1):9.

18. Jensen K, Ringsted C, Hansen HJ, Petersen RH, Konge L. Simulation-based training for thoracoscopic lobectomy: a randomized controlled trial. *Surgical endoscopy.* 2014;28(6):1821-1829.

19. Meyerson SL, LoCascio F, Balderson SS, D'Amico TA. An inexpensive, reproducible tissue simulator for teaching thoracoscopic lobectomy. *The Annals of thoracic surgery.* 2010;89(2):594-597.

20. Barsness KA, Rooney DM, Davis LM. Collaboration in simulation: the development and initial validation of a novel thoracoscopic neonatal simulator. *Journal of pediatric surgery.* 2013;48(6):1232-1238.

21. Kim GB, Lee S, Kim H, et al. Three-Dimensional Printing: Basic Principles and Applications in Medicine and Radiology. *Korean J Radiol.* 2016;17(2):182-197.

22. Chougule V, Mulay A, Ahuja B. Clinical case study: spine modeling for minimum invasive spine surgeries (MISS) using rapid prototyping. *Bone (CT).* 2018;226:3071.

23. Little BP. Approach to chest computed tomography. *Clin Chest Med.* 2015;36(2):127-145.

24. Abbas Q. Lung-deep: A computerized tool for detection of lung nodule patterns using deep learning algorithms. *Lung.* 2017;8(10).

25. Alsumrain M, De Giacomi F, Nasim F, et al. Combined pulmonary fibrosis and emphysema as a clinicoradiologic entity: Characterization of presenting lung fibrosis and implications for survival. *Respiratory Medicine.* 2019;146:106-112.

26. Falland-Cheung L, Pittar N, Tong D, Waddell JN. Investigation of dental materials as skin simulants for forensic skin/skull/brain model impact testing. *Forensic Science, Medicine, and Pathology.* 2015;11(4):552-557.

27. Merkel PA, Silliman NP, Denton CP, et al. Validity, reliability, and feasibility of durometer measurements of scleroderma skin disease in a multicenter treatment trial. *Arthritis Care & Research: Official Journal of the American College of Rheumatology.* 2008;59(5):699-705.

28. Jussila J, Leppäniemi A, Paronen M, Kulomäki E. Ballistic skin simulant. *Forensic science international.* 2005;150(1):63-71.

29. Kim T, Kim GB, Song HK, Kyung YS, Kim C-S, Kim N. Accuracies of 3D printers with hard and soft materials. *Rapid Prototyping Journal.* 2020.

30. Duan X, Wang J, Christner JA, Leng S, Grant KL, McCollough CH. Dose reduction to anterior surfaces with organ-based tube-current modulation: evaluation of performance in a phantom study. *American journal of roentgenology.* 2011;197(3):689-695.

31. Moloney F, Twomey M, James K, et al. A phantom study of the performance of model-based iterative reconstruction in low-dose chest and abdominal CT: When are benefits maximized? *Radiography.* 2018;24(4):345-351.

32. Mei K, Geagan M, Roshkovan L, et al. Three-dimensional printing of patient-specific lung phantoms for CT imaging: emulating lung tissue with accurate attenuation profiles and textures. *medRxiv.* 2021.

33. Hernandez-Giron I, den Harder JM, Streekstra GJ, Geleijns J, Veldkamp WJ. Development of a 3D printed anthropomorphic lung phantom for image quality assessment in CT. *Physica Medica.* 2019;57:47-57.

34. Zhang F, Zhang H, Zhao H, et al. Design and fabrication of a personalized anthropomorphic phantom using 3D printing and tissue equivalent materials. *Quantitative imaging in medicine and surgery.* 2019;9(1):94.

35. Craft DF, Howell RM. Preparation and fabrication of a full-scale, sagittal-sliced, 3D-printed, patient-specific radiotherapy phantom. *Journal of applied clinical medical physics.* 2017;18(5):285-292.